Numerical and Experimental Investigation of the Manufacturing Process of Ball Bearings Focusing on Enhancing the Aesthetics of the Outer Surface by Removing the Shining Band

by

Abdullah Alsairafi

Submitted in Partial Fulfillment of the Requirements

for the Degree of

Master of Science

in the

Mechanical Engineering

Program

YOUNGSTOWN STATE UNIVERSITY

May, 2018

Numerical Investigation of the Manufacturing Process of Ball Bearings Focusing on Enhancing the Aesthetics of the Outer Surface by Removing the Shining Band

Abdullah Alsairafi

I hereby release this thesis to the public. I understand that this thesis will be made available from the OhioLINK ETD Center and the Maag Library Circulation Desk for public access. I also authorize the University or other individuals to make copies of this thesis as needed for scholarly research.

Signature:

Abdullah Alsairafi, Student Date

Approvals:

Stefan Moldovan, Thesis Advisor Date

Kyosung Choo, Committee Member Date

Jae Joong Ryu, Committee Member Date

Dr. Salvatore A. Sanders, Dean of Graduate Studies Date

Abstract

Bearing supporting shoes play an important role in manufacturing bearings. A bearing shoe is the part that supports the bearing as its outer surface is machined. The work presented in this thesis was focused on numerical modeling of the process that creates the scars and scuff marks (shining band) created by the contaminants that are carried into the gap between the bearings and the shoes that support them. This phenomenon creates a shining band around the bearing which affects its aesthetics. In addition, additively manufactured carbon fiber filament was studied and examined to replace Tungsten Carbide (commonly called Carbide) as the material used to fabricate the shoes. The experimental part of this research included mechanical testing of the strength and wear rate of the 3D printed material used to create the shoes. The numerical part of this thesis included modeling an improved shoe by inserting a channel for clean fluid flow (water and emulsified oil mix) through the shoe to deflect the particles and prevent them from slipping into the film between the bearing and the shoe. A Computational Fluid Dynamics (CFD) software package (ANSYS FLUENT) was used to track the particles distribution in two and three-dimensional models. The results from CFD confirmed that steel particles can indeed be deflected using the method presented in this thesis.

Acknowledgements

The author thanks his parents and wife for the continuous support throughout his Master's degree studies. This work would not have been possible if it were not for their support and care.

The author also acknowledges and appreciates all the time and effort his advisor, Dr. Moldovan, has put forth in helping with this thesis. He continued to believe in the author and kept pushing him for better results.

A big thank you is in order for Youngstown State University machinists John Dodson, Steve Richards and Patrick Rovnak who helped with designing and testing the apparatus used in this thesis in the machine shop.

The author would also like to extend his gratitude to Youngstown State University's Center for Innovation and Additive Manufacturing and its manager, Jay Wargacki. Jay offered big help with the experimental part of this thesis with his expertise and knowledge in additive manufacturing.

Finally, the author is grateful for the funding of this research. This research was funded by Timken steel and Youngstown Business Incubator. Dr. Hazel Marie made it all possible, so a big thank you is the least the author can offer.

Table of Content

List of Figures

List of Tables

Chapter 1 Introduction

1.1 Description of the Engineering Problem

The process for fabricating bearings, regardless of the company that makes them, is very similar. In the later stages of manufacturing bearings, bearings have to be machined down to the desired outer and inner diameters to get the correct dimensions (1). During this process, some of the metal scrap particles get jammed between the bearing being ground and the shoes. The shoes are the parts that support the bearing during the machining process. In the bearing manufacturing process being investigated, two shoes are being used to support the bearing to be machined from the top. One is placed at 210˚ and the other is at 300˚ measured from the positive x-axis counterclockwise. The congestion of the contaminants within the bearing and shoes causes abrasion to the outer surface of the bearing. The scratches and scuff marks on the bearing cost money to resurface to a uniform surface in order to achieve the desired aesthetics. Multiple configurations of the shoes locations were tried without any success in preventing contaminants from entering between the shoes and the bearing. A solution to this problem is to be devised.

1.1.1 Tribological Aspect

The shoes under investigation in this research are made out of tungsten carbide (commonly referred to as carbide). A shoe made of carbide is durable but very costly. A carbide shoe can last to produce thousands of bearings without losing structure integrity or sacrificing precision and or accuracy. Carbide is very useful as a material to support rotating steel bearings. It has high hardness, strength and wear resistance over a wide

range of temperatures (2). Table 1 shows physical and mechanical properties of tungsten carbide.

Table 1 physical and mechanical properties of tungsten carbide (3)

Properties	Value
Tramsverse rupture strength (Mpa)	550
Young's Modulus (Gpa)	620
Vicker's Hardness (Gpa)	22
Shear Modulus (Gpa)	262
Poinsson's Ratio	0.18
Density (g/cm^3)	15.8
Electrical Resistivity ($x10^{-6}$ Ohmcm)	17
Specific heat (J/molK)	39.8
Melting point (˚C)	2870
Thermal Conductivity (W/mK)	63

The shining band phenomenon was reproduced using a steel cylindrical rod as the bearing and can be seen in Figure 1-1. In addition, a reproduced shoe made from carbon fiber filament by additive manufacturing can be seen in Figure 1-2

Figure 1-1 Shining band

Figure 1-2 Left and right shoes

However, the demand for bearings is less than it used to be and is always changing, therefore fabricating custom made carbide shoes is not feasible (4). A newer material that is less costly but without sacrificing the integrity of the process is to be found. Additively manufactured carbon fiber filament, a commercially available material, is to be considered as an alternative to the carbide. Two-dimensional drawings, provided by a bearing manufacturer, of the original shoes were converted into a three dimensional model using a computer aided design (CAD) package. Then prototypes of both the right and left hand shoes were fabricated using Polylactic Acid (PLA).

To reach the final version of the shoes, several prototypes had to be printed. According to Kruth and Leu, Rapid prototyping by additive manufacturing is a method used to quickly generate prototypes by the gradual creation or addition of solid material (5). Prototyping using additive manufacturing developed from the pre-commercial period in the late 1980s to 1998. At that time only a few additive manufacturing systems were not commercially available to the public. The surge in unit sales of the rapid prototyping units, which is what they were called then, started in 1993 (6).

Nowadays additive manufacturing machines, or simply 3D printers, are available to purchase through the World Wide Web or brick and mortar stores. The development of

the industrial additive manufacturing techniques such as Fused Deposition Modeling (FDM), Selective Laser Sintering (SLS) and Stereo-Lithography (SL). (6)

1.1.2 CFD Aspect

The presence of impurities and residuals in bearings lubricants can be found in several research articles. During normal operating conditions of bearings, contaminants can enter the lubricant film. Those particles have been extensively studied in applications where bearings are used as a mechanical component of a machine. They were not studied in the manufacturing process of bearings, however. Research about particles in bearings lubricant began more than ninety years ago with the work of McKee (7). He studied the presence of an abrasive material, like dust or solid particles attained from roads, in the lubricant of bearings and shafts and its effect on the performance of bearings in automobile engines.

Sharma and Hargreaves (8) tackled reducing wear and damage on bearings from solid particles by adding wear reducing material for contaminated lubricants that have solid impurities in them to help eliminating abrasions caused by the presence of particles. In his PhD dissertation, Sharma experimentally investigated claims by manufacturers of wear reducing material. According to that research, adding a proprietary material in lubricants will reduce wear on bearings. The conclusion of his research was that adding that material to the film thickness does not significantly reduce wear and abrasion. There are more studies by Roach (9), Elwell (10) and Wikström (11) about the presence of contaminants in the lubricant of different type of bearings. They mainly studied the entrance of foreign objects into journal bearings. Their studies included the study of self-propagating wear from contamination; however, there is not much literature available that

discusses the manufacturing process of bearings and how bearings get scuffed as they get machined because of the metal particles.

There is a study that discusses hydrodynamic bearings (12) scuffing failure as flash temperature reaches an assumed critical value. As particles get embedded between the bearing and the slider, shown in Figure 1-3, abrasion occurs. The continuous abrasion of the bearing causes it to eventually fail. A filtration system is needed to prevent the contaminations from entering the film amid the slider and bearing. It is impractical to create a filter that prevents all particles from entering the system therefore there will always be impurities in the lubricant. A criterion for the filter has to be determined however. If no particle bigger than the minimum allowable film thickness is allowed to enter the bearing clearance, no major damage is expected to occur (12).

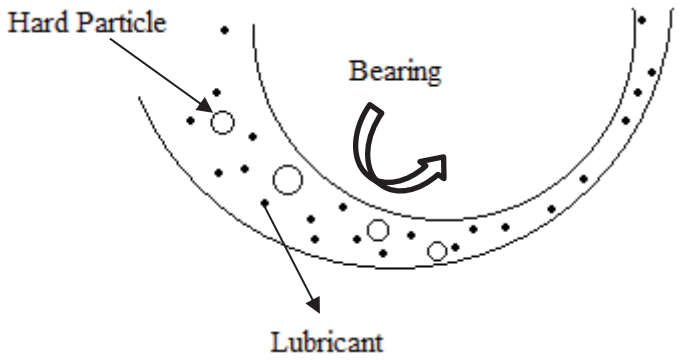

Figure 1-3 Particles entering the bearing clearance

Modeling flow that includes liquid and solid interacting with each other has never been easy. Du et al. (13) used the Volume of Fluid (VOF) method to create the mixture of liquid and gas flowing around spherical particles which resembled a fixed bed that has solid catalyst particles packed inside it while gas and liquid reactants flow across that packing section.

The VOF model can account for surface tension which can be the major force in the flow. Solving the continuity equation for the volume fraction of the different phases of the flow will result in known volume fractions of gas-liquid mixture at any location. In the above mentioned research paper, a solid spherical particle was fixed in place and made stationary and a mixture of fluid made of gas and liquid flowed across and around it.

Yan et al. (14)wrote about unsteady airborne pollutant transport within an aircraft cabin in a mock set up. They numerically simulated an environment similar to that of the aircraft in Fluent. The results from the experiment match the results from the numerical model set up in Fluent using the Species Transport model. Turning the species model on in Fluent allows for calculation of numerous species transport. The option of reacting or non-reacting flow can be chosen using the reactions command. A percentage mass fraction of each component can be assigned. In this research paper, 4.5L/min of carbon dioxide was injected into the system from what is modeled to be passengers but, in fact, are box-shape manikins. A diffuser was assigned as the boundary condition for mass flow inlet of air. An exhaust grill was assigned to be the outlet of the mixture of air and carbon dioxide. This paper confirms the possibility to use species transport to model gas pollutants.

Another possible way of modeling contaminants would be through using the Discrete Phase Model (DPM). In a journal about ash deposition for co-combustion of meat and bone meal (MBM) with coal in a fired utility boiler, Taha et al (15). mention the combustion of solid fuels and the deposition of ash on the surface of the heat exchanger. The properties of those particles are calculated through thermodynamic equilibrium for

oxidizing and reducing conditions. Both MBM and coal particles were injected as a mixture. A certain number of particles was picked and the particle velocity was calculated over time step to obtain the particles displacement. A graph of mass fractions of coal particles after combustion along a plane in the center of the boiler's geometry is shown. The graph shows where the concentration of the ash is and the region the ash doesn't reach. This is done using different percentages of co-firings of coal and MBM. Results from CFX in the article show residence time of particles which is not very helpful in quantifying particles count or density in certain regions at certain times.

Windblown dust transport from a mine tailings impoundment was modeled and simulated by Stovern et al. (16). They used FLUENT species transport models and discrete phase model to simulate wind that carried contaminants away in the air. Tailings are the left over material from processing ores (17). Those left over materials contain lead and arsenic contaminants, which if inhaled, pose serious health issue. A tailings impoundment (pond) is reservoir for processed material (17). The tailings impoundment simulated in this journal was the Iron King Mine tailings in Dewey-Humboldt, Arizona. Local weather patterns and landscape features were incorporated in the CFD model to accurately simulate the problem. Boundary conditions for this model include inlet mass fraction, inlet mass flux, inlet direction specification and boundary species fractions specifications. Very fine particles were modeled as aerosol which is a fluid. It is assumed that the solid arsenic and lead particles are so fine and small that they float as a fluid carried by wind. Therefore, they were included in the species transport model. Larger particles were injected by the discrete phase model.

The discrete phase model's biggest flaw is that it only tracks the trajectory and location of the injected particle. In the previous journals, DPM was used to model the dispersion of dust, aerosols and coal particles and track there location. However, there is no method for quantifying the particles or showing contours of the density of the particle in a certain region. DPM in ANSYS shows only residence time in certain locations.

Chapter 2 Experimental Procedure

For this part of the thesis, a three-dimensional model of the shoe was built using 2016 x64 SolidWorks CAD package. The model was created from two-dimensional drawings supplied by the steel bearing manufacturing company. The three-dimensional model was then exported into an STL extension format to be additively manufactured. Different types of materials were used for prototyping. However, the material used to 3-D print the shoe used in mechanical testing of this thesis is ONYX ™. The mechanical properties of this material can be seen in Table A.1 in the appendix. Multiple iterations of the model were fabricated for testing and collecting empirical data.

2.1 Geometry

The geometry for the shoes used in the manufacturing process of the bearings was created using the above-mentioned software. They were drawn in three dimensions and then converted back into a two-dimensional drawing. This was done to compare the two-dimensional drawing provided by the manufacturer to the one generated in SolidWorks and check for accuracy. Figure 2-1 shows both the right hand shoe and the left hand shoe both in three dimensions and as two-dimensional drawings.

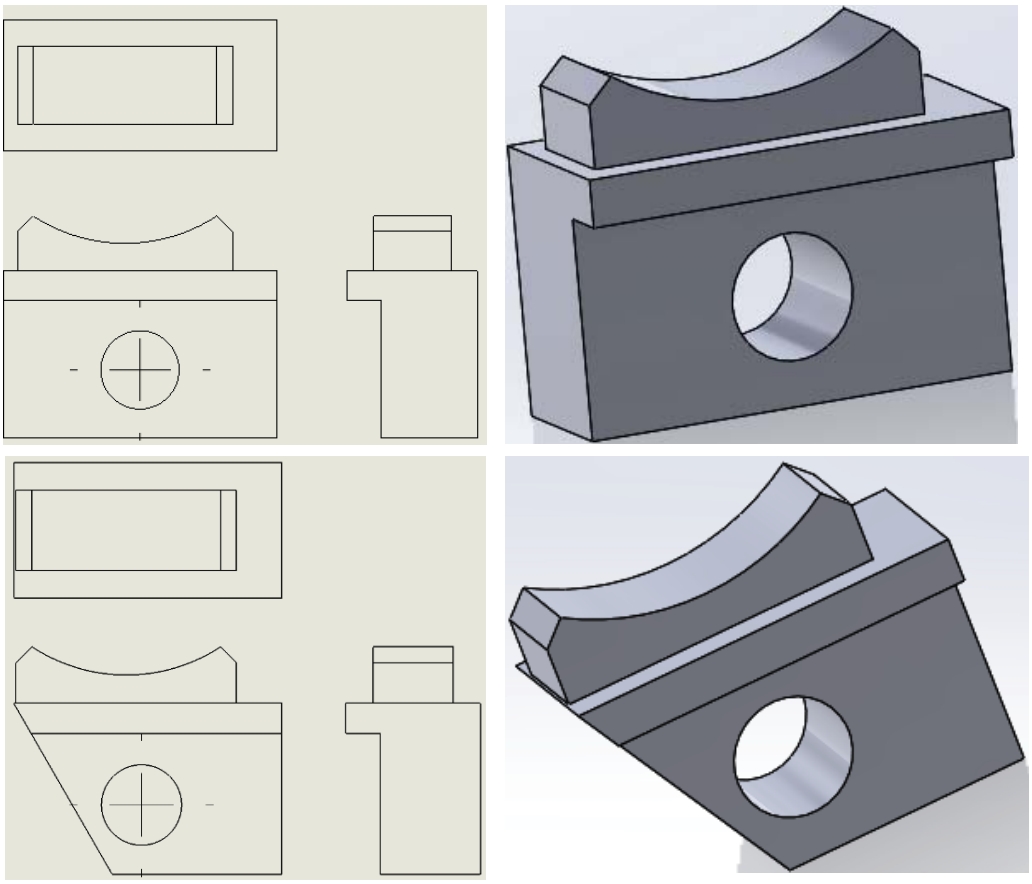

Figure 2-1 Two and three-dimensional models of the left shoe (top) and right shoe (bottom)

2.2 Additive Manufacturing

2.2.1 Standard Shoes

The shoes, both right and left, shown in Figure 2-2, were first additively manufactured using Polylactic Acid (PLA) in the CREATORBOT 3D Pro Series II which can be found in Figure 2-3. PLA was used because it is affordable, odorless and warps less. It is good for fast and easy prototyping (18). The first iteration of the 3D printed shoes was to make sure the shoes were drawn correctly.

Figure 2-2 3D printed shoes, first iteration

The CREATORBOT 3D Pro Series II is one of the biggest 3D printers in its class with 12”x12”x18” print volume and a maximum resolution of 40 µm. it uses Fused Filament Fabrication technology (FFF). It has dual heads with a nozzle temperature of 170˚c to 260˚c (19). As can be seen from Figure 2-2 the resolution of the printed shoes are very low. Therefore, another iteration was executed.

Figure 2-3 CREATORBOT 3D Pro Series II

For the second iteration of the additive manufacturing of the shoes LULZBOT Taz 6 was used. It features automatic bed leveling and self-cleaning. The material used for this print was Bridge Nylon by Taulman 3D which is a Nylon co-polymer that was also

manufactured by LULZBOT. The settings of the print were refined by increasing the resolution. The LULZBOT Taz is presented in Figure 2-4.

Figure 2-4 *LULZBOT* Taz 6 3D printer

The final iteration of the additively manufactured shoes was done using a higher end 3D printer. The printer's manufacturer is Markforged and the model name is "The Mark Two". It is able to manufacture sturdy materials like carbon fiber, fiberglass and Kevlar. This printer and material were used because they combine the affordability, strength and durability required to withstand the loading applied during the machining process of bearings.

Figure 2-5 3D printed shoe, final iteration

Figure 2-5 shows the final set of shoes, which were printed a total of four copies.

2.2.2 Shoes with Fluid Channel

A shoe with clean water injection channel was first modeled in SolidWorks and then additively manufactured. The shoe has a circular cross section at the base and lofts to a rectangular cross section at the top, which should evenly pump the lubricant to deflect the particles away from the shoe. The 3D model can be seen in Figure 2-6. Another figure that illustrates the bottom of the shoe with the circular hole can found in Figure A.1 in the appendix.

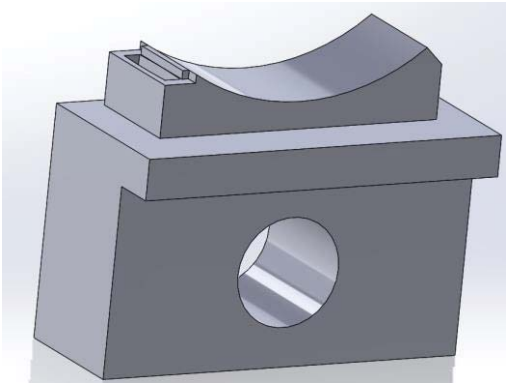

Figure 2-6 Shoe with a fluid injection channel

The shoe in Figure 2-6 was additively manufactured in the same manner as the final iteration of the standard shoes. They were printed using the Markforged printer and Onyx carbon fiber filament material.

2.3 Experimental Setup

The shoes were tested for wear rate and strength. The first test was performed using the Instron machine to determine the static load that the bearing can withstand. The results showed how the shoes react to static loading and how that affects the manufacturing process. The second test was the wear rate and aesthetics test. The results from this test indicate how the material affects the outer raceway of the bearing and how the shoes wear with time.

2.3.1 Static Loading Test Setup

The shoes fabricated from ONYX™ carbon fiber filament was placed on a flat surface at the center of the machine. A cylindrical steel (steel grade and properties can be found in

Table A.2 in the appendix) rod that mimics the size of a bearing slowly pressed against the curve of the shoe with an incremental force. The loading starts from zero force and then the compressive load increased gradually at a rate of 0.25mm/min until fracture was achieved. This test was done on both the left and right hand shoes. Figure 2-7 shows the loading until fracture for the left and right shoe. Another criterion to evaluate the shoe was the deflection under a given load. Shoes should deflect no more than 0.25 mm under the force applied in the manufacturing process. If the deflection is greater than 0.25 mm, the material would not be useful for this application as excess deflection could result in uneven machining. The grinding force used for the bearings machining process is 150N. Therefore, the data was recorded specifically at this point to

determine the value for deflection in the shoe. The data acquired from the Instron machine's static loading test showed the deflection of the shoes. And is presented in Figure 4-1 in the results and discussion chapter of this thesis. The stress and strain curve for both of the shoes can be found in the results chapter as well in Figure 4-2.

Figure 2-7 Loading of the left and right shoes

2.3.2 Wear Rate and Aesthetics Test Setup

For the wear rate test, both shoes are weighed before and after the test. The fixture pictured in Figure 2-8 was designed to fit on the lathe machine. As can be seen in the Figure 2-8, the shoes are pinned to fork joints. The pins allow for planar rotation while the slot prevents out of plane rotation. The fork joints are pulled toward each other with spring. This generates a moment on the fork joints that translates to the grinding force of 150N applied to bearings in manufacturing process. A cylindrical steel rod is then put in the chuck of the lathe. The rod mimics the bearing being machined. The lathe is switched on and set to rotate at 900 rpm which is similar to the rotational speed the used in the manufacturing process. Clean coolant made of water and oil (95% water to 5% oil) is

discharged on the rod and shoes as the rod rotates. The coolant also acts as a lubricant to reduce friction. The cylindrical rod was sanded to a smooth finish so that any abrasions can be easily sighted with naked eye or under the microscope. Three different experiments were done and procedure for each one of them is described in the next sections.

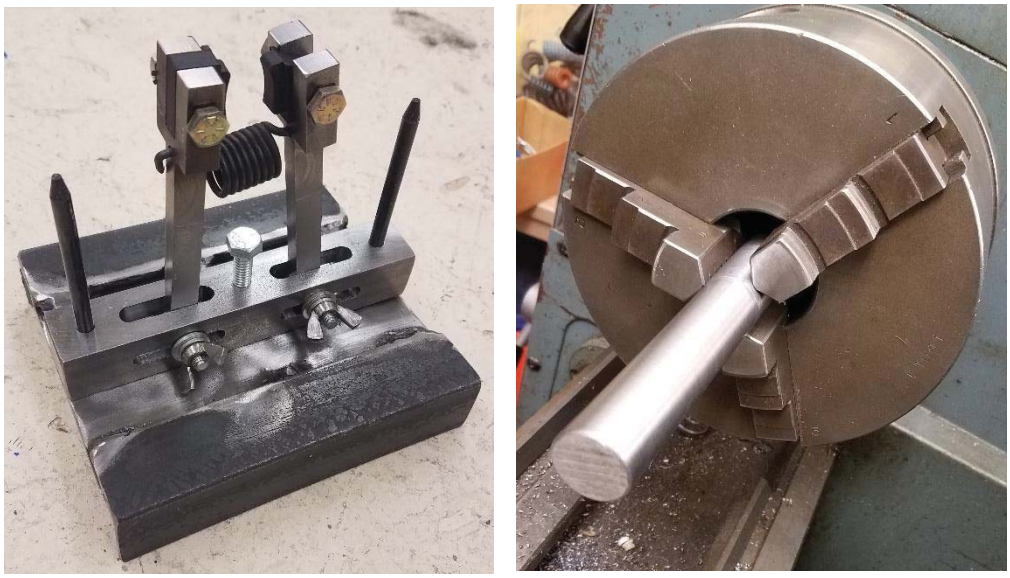

Figure 2-8 Experimental setup

2.3.2.1 Dry Run Setup

In first experiment, the shoes were pinned in place as shown in Figure 2-8. The lathe was run with no coolant discharge on the shoe and cylindrical rod. This was done to see how the shoes surface that is in contact with the rod wears. The test was run for 30 minutes. The results of this experiment can be found in chapter 4.

2.3.2.2 Clean Wet Run Setup

The second experiment was done with clean coolant pumping through the injection channel of the left shoe. The flow rate of the coolant through the shoe was 1.2 liters/min. This test was run to see how the shoes wear under lubrication. The rotational speed of

this test was also 900 rpm. The duration of the test was 30 minutes. The results from this test are reported in chapter 4.

2.3.2.3 Dirty Wet Run Setup

The third and last experiment was done with clean coolant pumping through the injection channel of the left shoe and, in addition to that, steel powder was added throughout the process. This test was run for 30 minutes. Steel powder was added at 16.5 g/min. therefore, a total of 495 grams of steel powder was added to the run. This step was included to see the effect of the clean coolant pumping through the injection channel on the dirt entering the system. This simulates the actual machining of the outer ring to reproduce the shining band phenomenon on the steel rod.

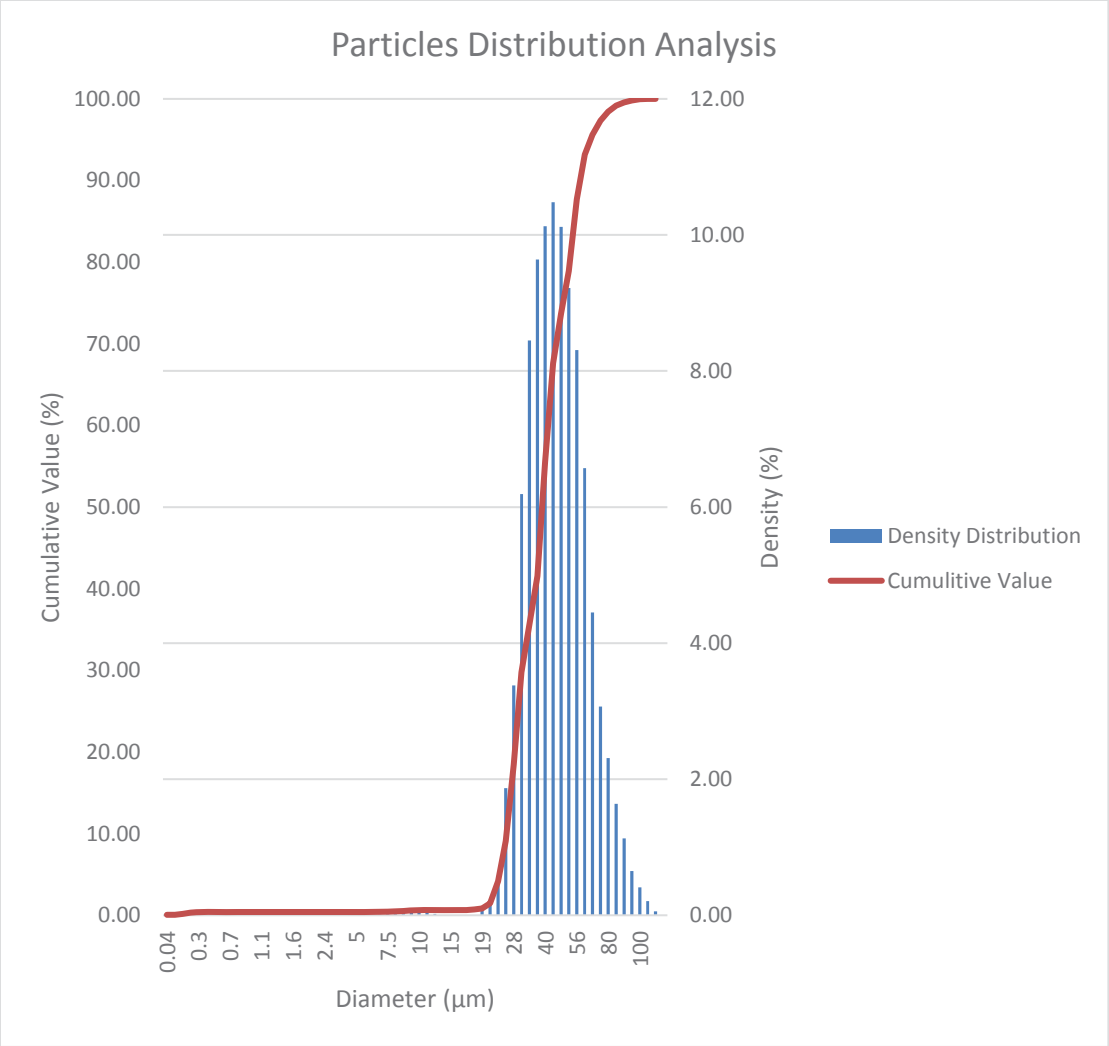

Figure 2-9 Distribution Analysis of the steel powder

The steel particles went under a distribution analysis to get a general idea of the size of the particles used. The results of the distribution analysis which was done to five samples pulled from the same pool of steel powder shows the particles diameter range from 0.04 µm to 2500 µm. The graph in Figure 2-9 shows more details about the samples.

Chapter 3 Numerical Model

Numerical modeling of steel particles flowing in the water/oil mix can be done by approximating the small steel particles as a liquid by giving them fluid properties and letting them mix, as a fluid, with the emulsified oil mixture. This way, solving for the volume fraction for the steel impurities by solving the continuity equation will render the locations where the contaminating particles are inhibiting.

3.1 Software

For the numerical model, the ANSYS software package was used. ICEM CFD was used to construct the geometry of the model. In addition, it was used to generate and control the unstructured mesh created for the model. ICEM CFD was used because it allows the user to freely control what type of mesh and spacing between elements. Two and three-dimensional models were devised using this package. ANSYS Fluent was used to run two and three-dimensional simulations of the shoe, bearing and fluid system. Fluent was used to simulate both the fluid flow of the original show model and the shoe with the fluid injection channel.

3.2 Geometry

3.2.1 Geometry of the Original Shoe

The bearing manufacturing process that generates the shining band was modeled in ANSYS. It consists of three different components, a bearing, a shoe to support the bearing, a small gap between the shoe and the bearing (one tenth of a thousand of an inch or 2.54×10^{-6} m) and a fluid that flows in the system. The manufacturing setup has two shoes supporting the bearing. As an approximation and for simplicity of creating and

running the model, only one shoe is used here in lieu of the original two shoes. Also, this was done to model the worst case scenario of steel particles entering between the bearing and shoe. This phenomenon happens to the left shoe more than the right shoe. Modeling the right shoe will not generate a better representation of the shining band phenomenon. Therefore, the right shoe was eliminated from the modeling.

3.2.1.1 Two-Dimensional Geometry

At first, a two-dimensional model was created to perform the simulations using both the Volume of Fluid (VOF) and Species Transport methods. These methods use different formulations, as the VOF method uses volume fractions while Species Transport uses mass fractions; however, the same geometry is used for both. A two-dimensional center plane cut of the three dimensional model was taken for this simulation. It was used for the purpose of saving computation time as the three dimensional model is much larger and would require exponentially more time to run. The simple two-dimensional model is shown in Figure 3-1. It should be noticed that, as mentioned in the geometry introduction, there is a small gap between the shoe and the bearing. The bearing is a complete circle and the shoe overlaps in the regions shown by arrows in Figure 3-1.

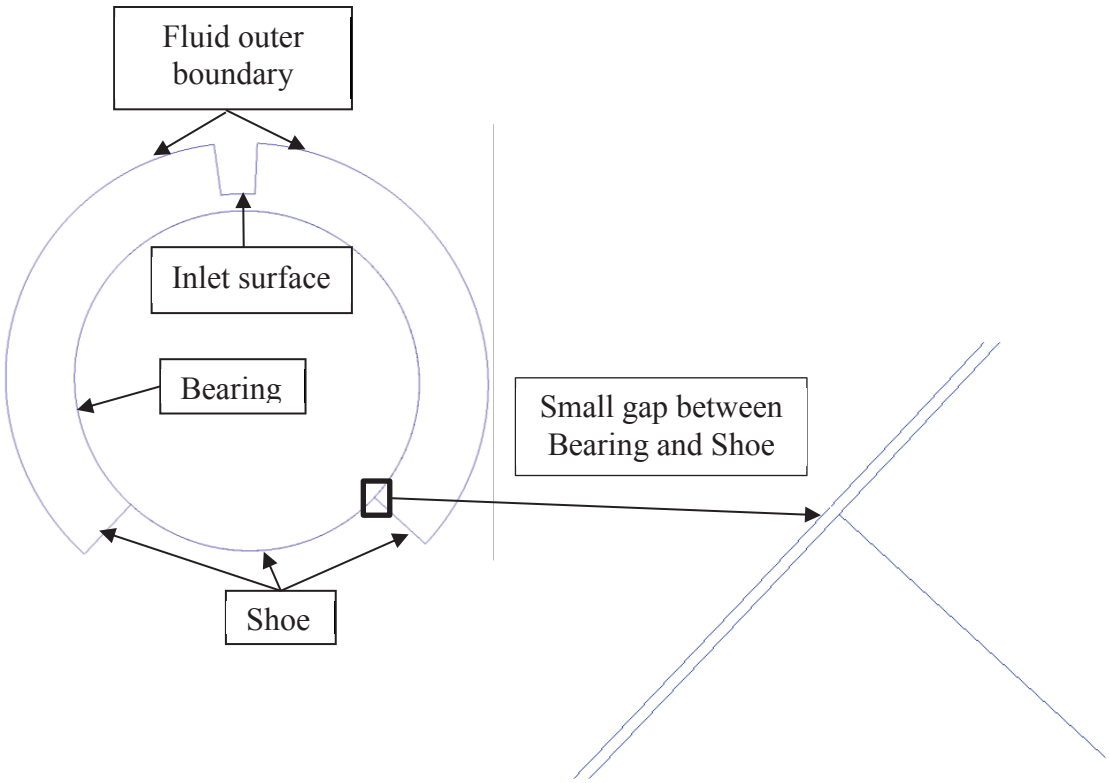

Figure 3-1 Geometry of the two-dimensional model

3.2.1.2 Three-Dimensional Geometry

The two-dimensional drawing of the system was drawn at first and then it was extruded to create the cylindrical shape of the bearing. Figure 3-2 shows an isometric view of the model. Also Figure 3-2 more isometric views of the geometries with the fluid outer boundaries can be found in Figure A.2 in the appendix.

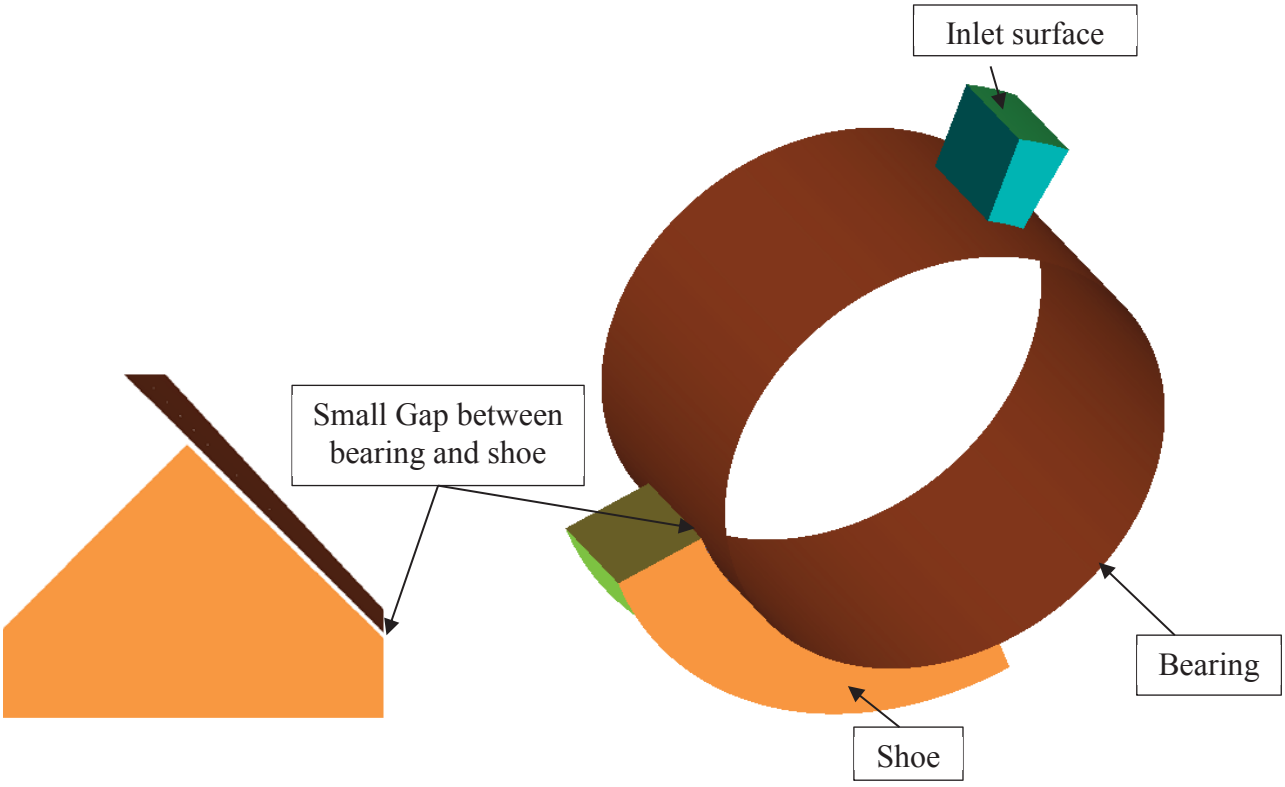

Figure 3-2 Three-dimensional geometry, isometric view

The three dimensional model consists of three different components, a rotating part, a fixed part and the fluid. The rotating component is the bearing itself. It is the brown component that can be seen in Figure 3-2. The second part is the fixed component which is the shoe the bearing rests on while being machined from the top. It is labeled as shoe. The last component is the fluid domain that is injected from the inlet and runs between the bearing and the shoe and everywhere else in the domain.

3.2.2 Geometry of the Shoe with the Injection Channel

The original shoe design was replaced with a new design that allows clean coolant to be pumped under the frontal region of the shoe. The new shoe was first modeled in SolidWorks 2016 x64 edition. The model has an orifice, or an injection channel, at the left side of the shoe that is used to inject water to deflect particles coming in from the left

side of the shoe. The 3D CAD model of the shoe can be seen in Figure 3-3. Also in similar manner to the previous three dimensional model of the original shoe, the shoe with fluid injection channel was imported into ICEM CFD for meshing. The geometry of the model can be found in Figure 3-4

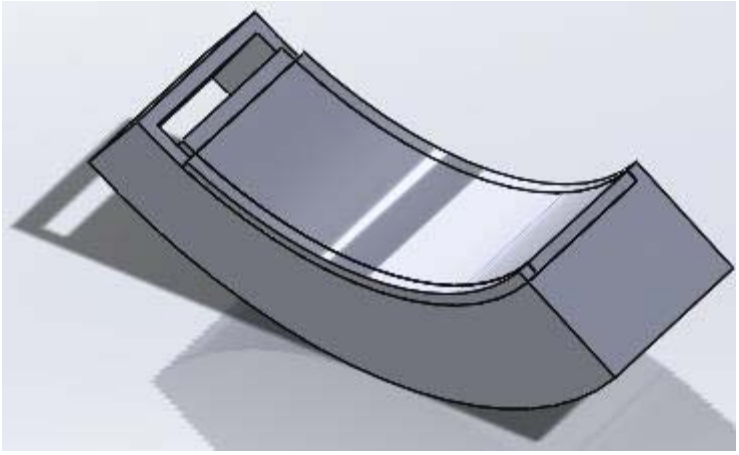

Figure 3-3 CAD model of the shoe with fluid injection channel

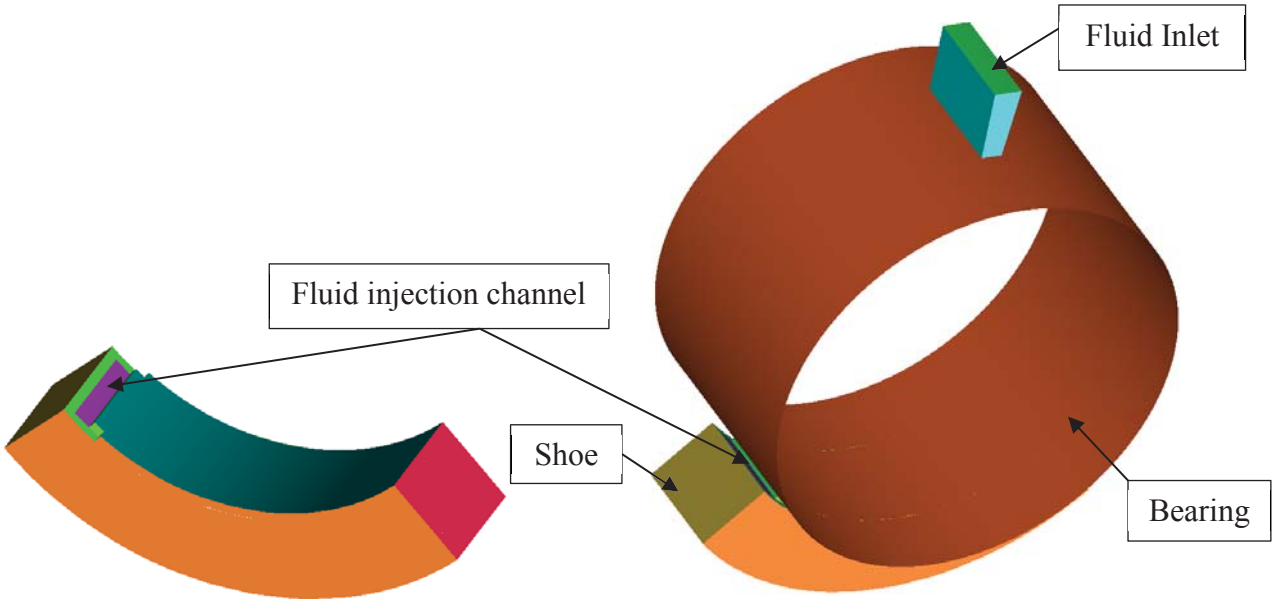

Figure 3-4 3D model of the shoe with the fluid injection channel

The part shown in Figure 3-4 is partial of the model. The rest of the model was hidden for visual purposes. The rest of the model is similar to the model of the original shoe.

There is a bearing that rests on the shoe and there are pressure outlets on the left and right sides and the outer side of the model. After building the model, everything was imported to ICEM to be meshed.

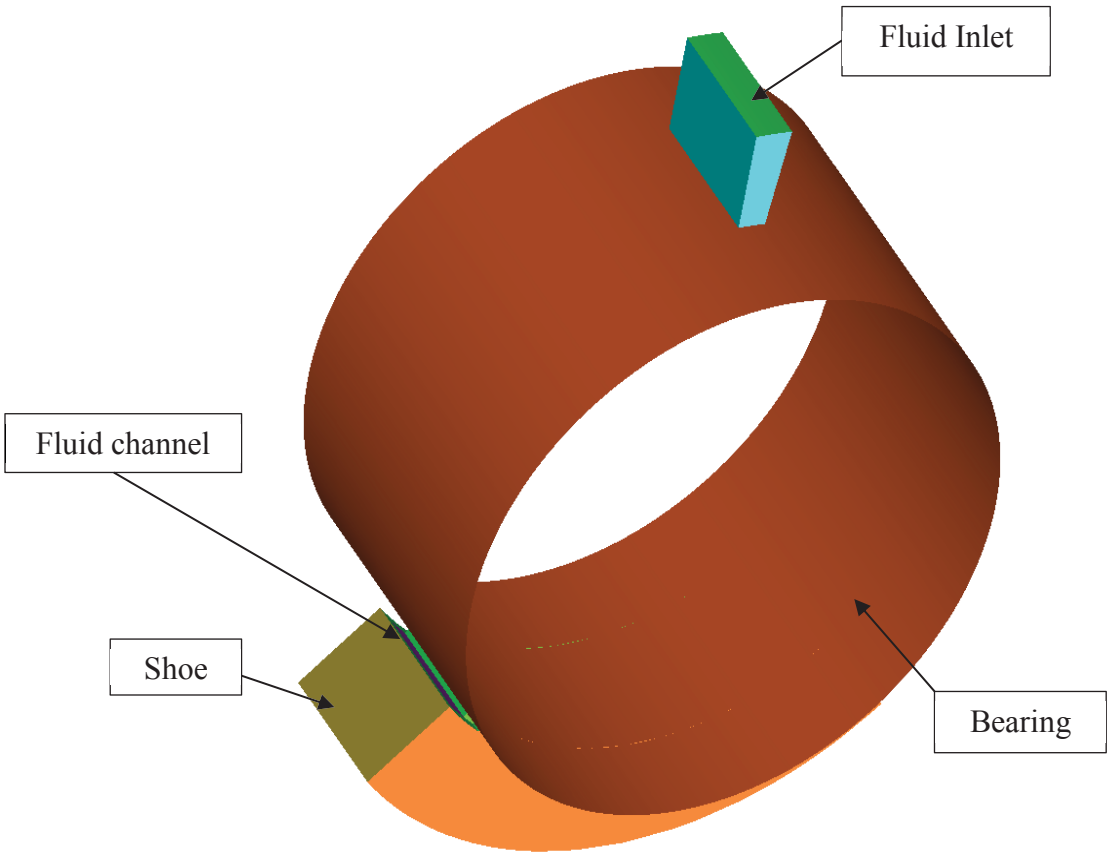

Figure 3-5 Boundary conditions of the model with the injection channel

3.3 Mesh

3.3.1 Mesh of the Original Shoe Model

Two and three-dimensional meshes were created. A combination of Bigeometric, Geometric 1 and Geometric 2 mesh laws are used to create a fine mesh with high quality

elements. Having high quality elements in addition to fine mesh results in less computation times for the mesh.

3.3.1.1 Two-Dimensional Geometry Mesh

After creating all the geometry lines and curves in ANSYS ICEM, for the two-dimensional mesh, a 2D planar block was initialized using the blocking feature. The blocking feature in ICEM creates a projection based mesh generation environment (20). This step is important to create and manipulate element shapes and sizes. After creating the 2D planar box, the initial block was split using the O-grid block feature. An O-grid block perfectly meshes circular geometry (21). After that, the blocks were split so that there is an edge for each corresponding curve. Some unnecessary blocks were removed as well. The final blocking shape is shown in Figure 3-6. The resulting mesh of this model has a quality of 1. All elements created in this model are rectangular elements with a quality of 0.95 to 1. Elements did not have any skewness or wide angles.

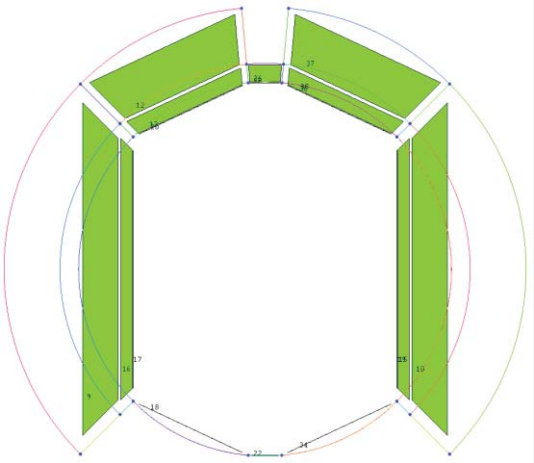

Figure 3-6 2D blocks

After creating the blocks all edges were associated to their corresponding curves to define the domain of the model. Next, all edges were assigned a mesh law, number of nodes, spacing between nodes and ratio of growth. Two types of mesh bunching laws

were used for this model, a Geometric and a BiGeometric meshing laws. In a BiGeometric law, according to ANSYS ICEM CFD 2016 manual, curves are defined by nodes points and cumulative distance. The node points correspond to the x-axis. The cumulative distance corresponds to the y-axis. The spacing and ratio create a linearly spaced points at certain ratio. Of the nodal points are not enough, the software ignores the ratios input by user (20). A Geometric bunching law uses spacing to set the first distance from the beginning of the edge. Then the remaining nodes are spaced with a constant growth ratio. This meshing law is described by the following equation:

$$S_i = \frac{R-1}{R^{N-1}-1} \sum_{j-2}^{i} R^{j-2} \quad (20)$$

Where S_i is the distance from the beginning of the edge to node i, R is the ratio and N is the total number of nodes. The ratio R is limited by $0.25 < R < 4.0$.

Figure 3-7, shows the node distribution. It should be noted that even though only one edge is marked, all properties of that edge were copied to all parallel edges. The parameters applied to each edge can be found in Table 2Table 2 node distribution and properties. It should be noted that the letter g refers to the elements in the small gap between the bearing and the shoe. The total number of nodes for this model is 144,592 nodes and the total number of elements is 143,200 elements.

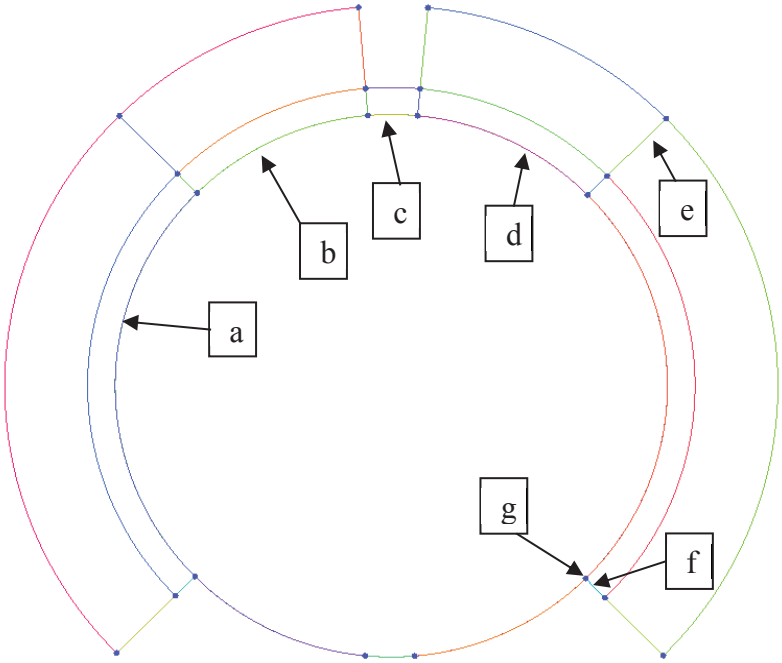

Figure 3-7 2D model node distribution

Table 2 node distribution and properties

	Mesh Law	Number of Nodes	Spacing 1	Ratio 1	Spacing 2	Ratio 2
a	Geometric 1	481	8.2814e-4	3	0	2
b	BiGeometric	61	0	2	0	2
c	BiGeometric	17	0	2	0	2
d	BiGeometric	61	0	2	0	2
e	BiGeometric	41	0	2	0	2
f	Geometric 2	81	0	2	1e-5	1.3
g	BiGeometric	11	0	2	0	2

The resulting mesh can be seen in Figure 3-8. A zoomed in view with more detail of the mesh can also be seen in the same figure.

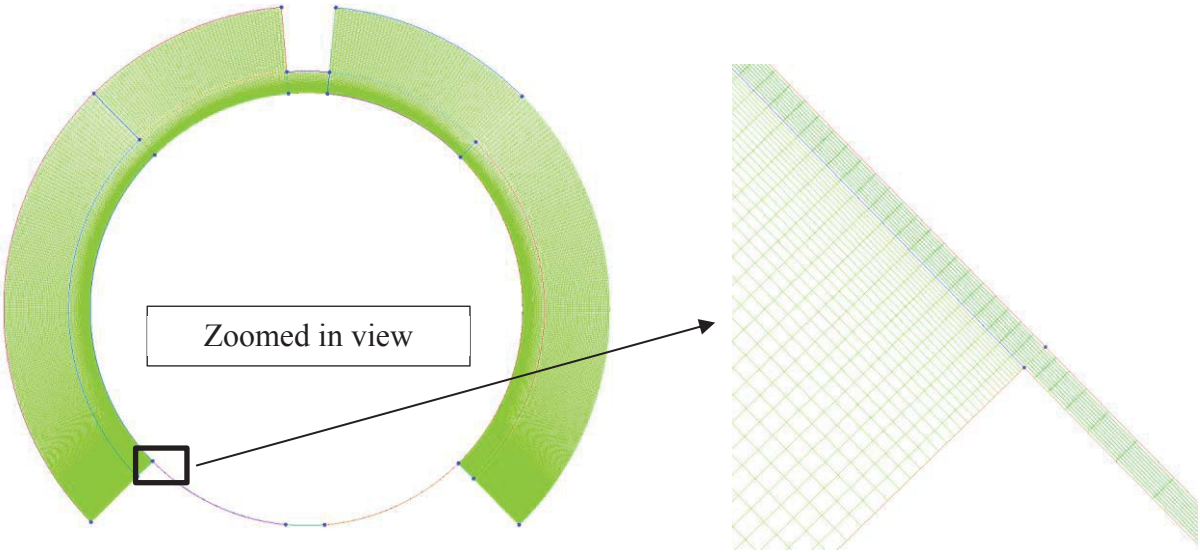

Figure 3-8 2D modelmesh

3.3.1.2 Three-Dimensional Geometry Mesh

The mesh of the three dimensional model of the original shoe was constructed in a similar way to the two-dimensional model. Additional steps were taken to account of the depth of the model. Figure 3-9 shows the geometry lines with the O-grid blocks marked in green.

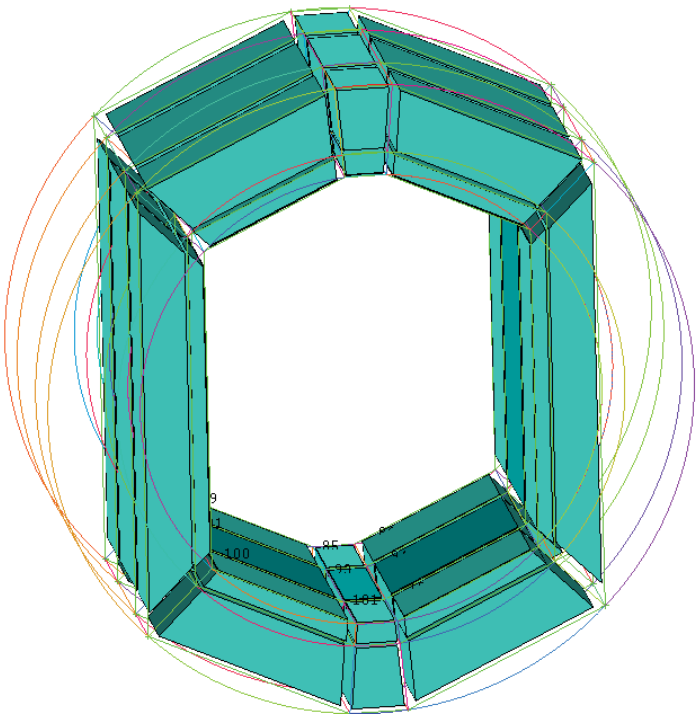

Figure 3-9 3D model, geometry lines and blocks

Just like the two-dimensional model, the three-dimensional one has elements distribution as shown in Figure 3-10 and Table 3. The only difference here is the addition of the z-axis. There are 69 nodes in the z direction. The first segment of the model has 20 nodes, the second segment has 29 nodes and the third and last segment has 20 nodes. The edge parameters were copied to all parallel edges. Spacings and ratios were assigned to make the mesh finer in regions of interest and then fade out in regions of less interest. It should be noted that the letter g refers to the small gap between the bearing and shoe which has 7 nodes and 6 elements. This model has a total number of nodes of 2,225,880 and 2,152,848 elements.

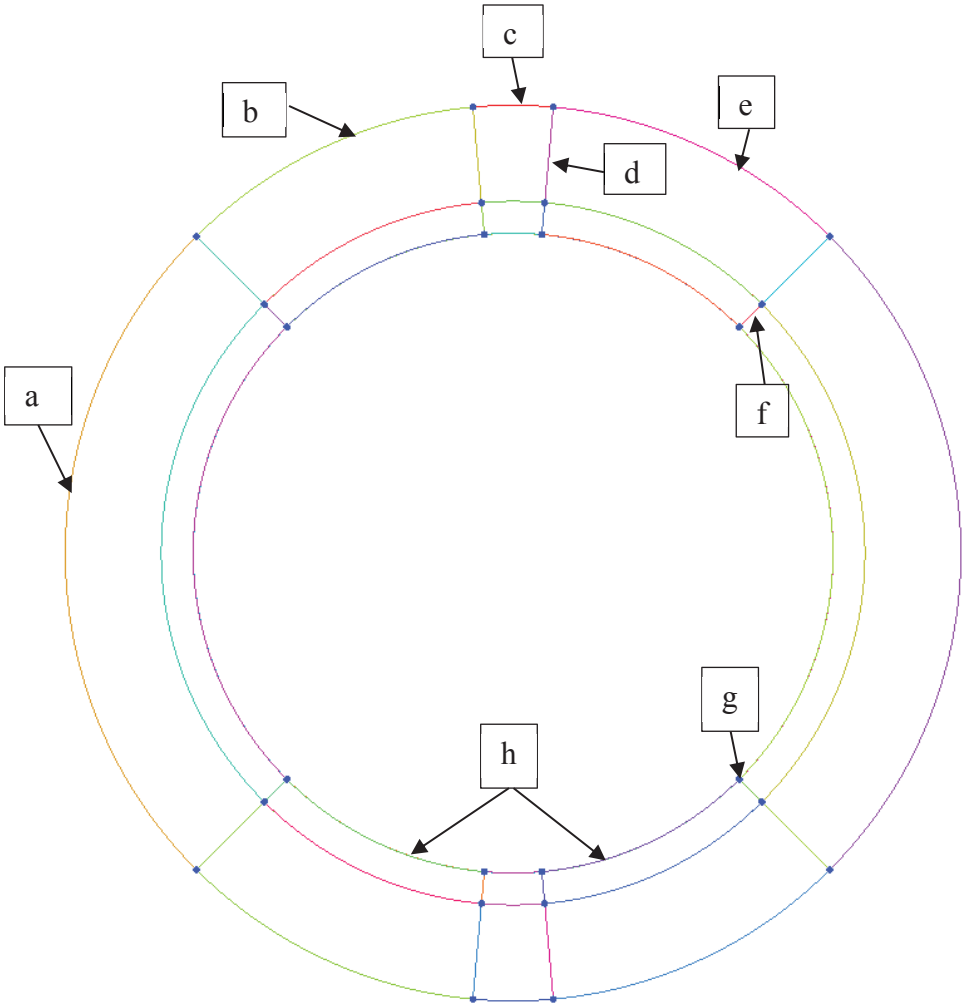

Figure 3-10 3D model node distribution

Table 3 node distribution and properties for the three dimensional mesh

	Mesh Law	Number of Nodes	Spacing 1	Ratio 1	Spacing 2	Ratio 2
a	BiGeometric	130	4.9275e-5	1.1	0	2
b	BiGeometric	39	0	2	0	2
c	BiGeometric	12	14	2	14	2
d	BiGeometric	26	0	2	0	2
e	BiGeometric	39	0	2	0	2
f	Geometric 2	39	0	2	2e-5	1.3
g	BiGeometric	7	0	2	0	2
h	BiGeometric	39	0.01	1.5	2.7261e-5	1.1

The mesh is presented in Figure 3-11. The mesh has a moderate density in regions of less interest and higher density in regions of interest which would render more accurate

results. A more zoomed in model and an isometric view of the model are shown in Figure 3-11 and Figure 3-12. The mesh is orthogonal

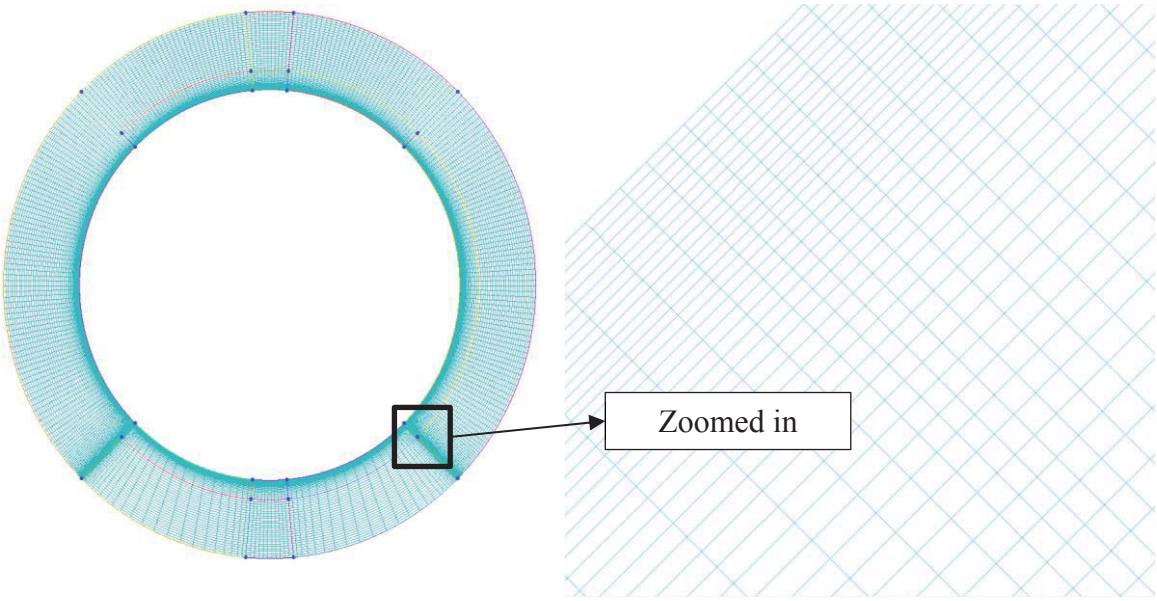

Figure 3-11 3D model mesh, center plane cut

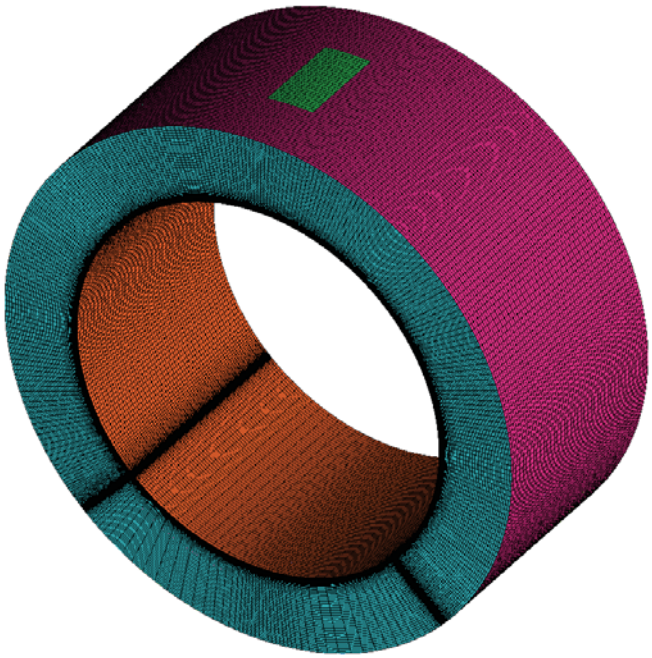

Figure 3-12 3D model mesh, isometric view

3.3.2 Mesh of the Model with the Fluid Injection Channel

Like the two and three-dimensional models of the original shoe, the three dimensional model with the fluid injection channel was meshed using a 3D bounding block. The bounding block was then split using the O-grid mesh to produce an orthogonal mesh. Figure 3-13, Figure 3-14 and Table 4 show the geometry lines as well as the blocks and the node distribution in ICEM.

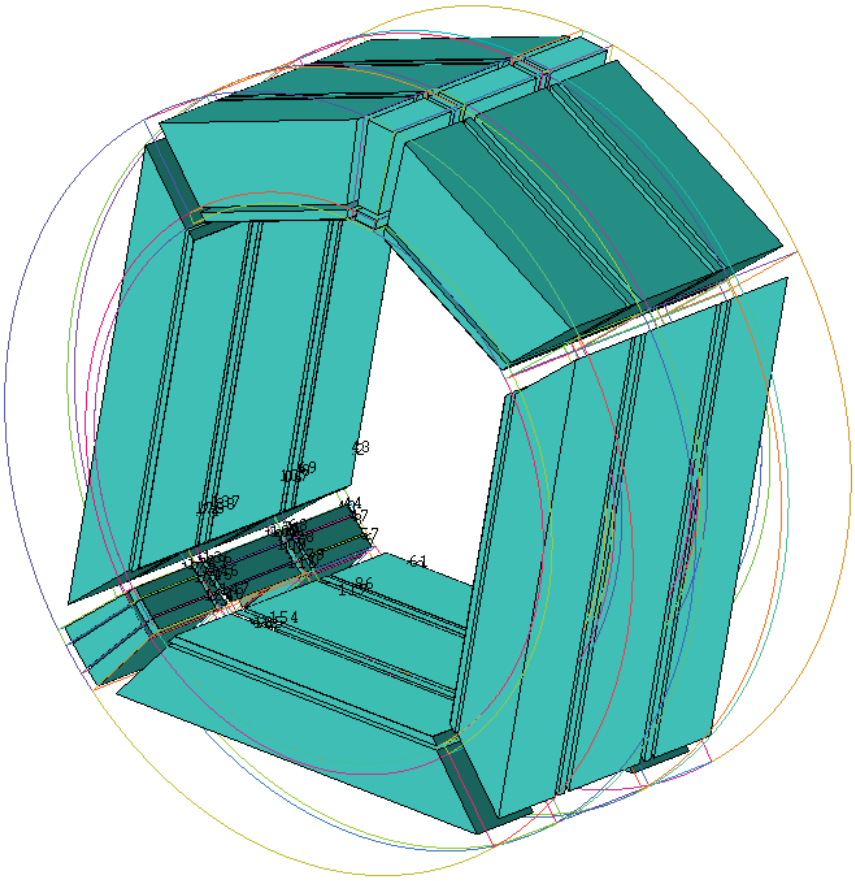

Figure 3-13 3D model of the fluid injection channel, blocks

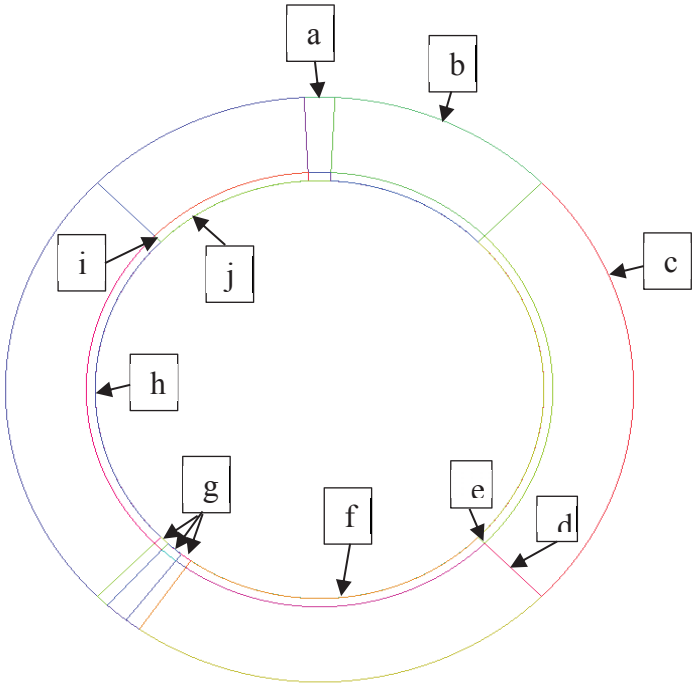

Figure 3-14 3D model with the fluid injection channel, node distribution

Table 4 node distribution for the model with the injection channel

	Mesh Law	Number of Nodes	Spacing 1	Ratio 1	Spacing 2	Ratio 2
a	BiGeometric	6	0	2	0	2
b	BiGeometric	42	0	2	0	2
c	BiGeometric	61	0.000306108	1.3	0.000225079	1.3
d	BiGeometric	51	0	2	0	2
e	BiGeometric	11	0	2	0	2
f	Geometric 1	91	8.47565e-5	1.3	0	2
g	BiGeometric	39	0	2	0	2
h	BiGeometric	101	4.9119e-5	1.1	0.000389696	1.1
i	Geometric 2	31	0	2	2.5e-7	1.3
j	Bigeometric	42	0	2	0	2

It should be noted that the letter e refers to the elements in the small gap between the bearing and the shoe. That gap has 11 nodes and 10 elements in it. All of these nodes properties were copied along all parallel edges. Also it should be noted that along the extrusion of the model in the z-direction, there are a total of 131 nodes. Therefore, there are a total of 3,714,461 nodes and 3,619,020 elements. Figure 3-15 shows an isometric

view of the mesh. Figure 3-16 shows the detail of the mesh around the injection channel and gap between the shoe and bearing.

Figure 3-15 3D model with the fluid injection channel, mesh isometric view

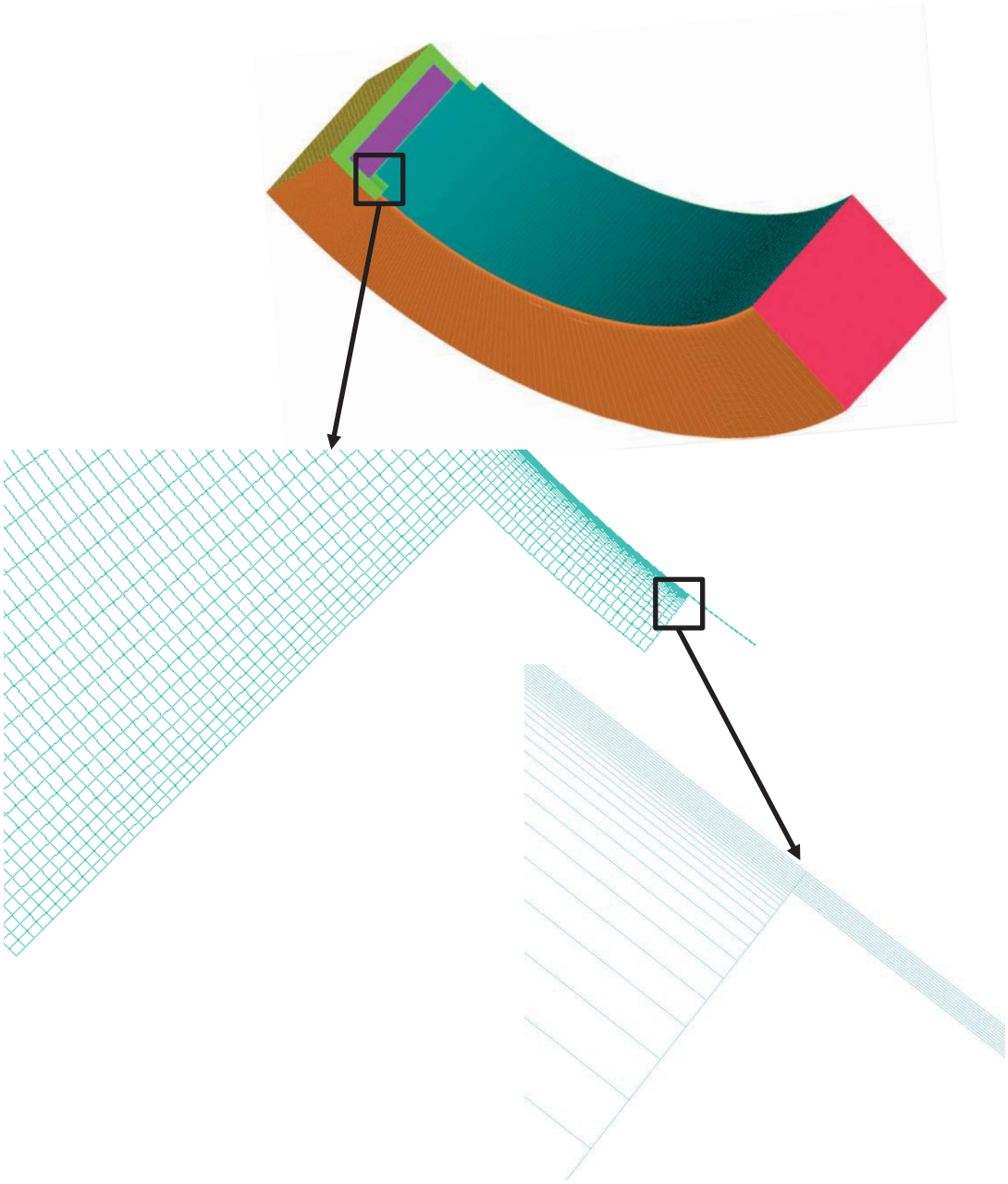

Figure 3-16 3D model with the fluid injection channel, a front detail view of the mesh

3.4 Computational Setup

For all of the models, two and three-dimensional, the solver chosen to run and compute the meshes is Fluent. The meshes were saved with a .msh file extension in

ICEM to be read by ANSYS FLUENT. After reading the meshes in ANSYS FLUENT, they were scaled to their true size.

The gravity term was included in the calculations. The magnitude is 9.81 m/s^2 and the direction is in the negative y-axis direction. Gravity is needed because fluids with different densities will separate because of the buoyant forces. Buoyancy force ($F = \rho V g$) (22) is dependent on fluid density(ρ) in kg/m^3, volume of the fluid in m^3 and standard gravity 9.81 m/s^2. As can be seen later, steel was modeled as a fluid and was assigned a certain density and viscosity and therefore, gravity was important to be included in the calculations. The solver was chosen to be pressure based. The pressure based solver is used in cases of incompressible flows. The flow was chosen to be steady-state. A steady flow refers to inflow or outflow conditions that do not change with respect to time. In addition, if the fluid properties inside a control volume don't change, the flow can be characterized as a steady state flow (23). In addition, a steady state configuration was chosen for this model because the process is repeated over and over again; meaning that bearings are machined one after the other. Therefore, the type of fluids flowing in the domain don't change and the size or operating conditions don't change either. Hence, a steady state solution was devised.

Like the two-dimensional model, the gravity term for three-dimensional models of the original shoe and the shoe with the injection channel, was also included in the calculations with the same parameters and properties. In addition, steel was also modeled as a fluid and was assigned a certain density and viscosity. The solver was chosen to be pressure based because the flow is still incompressible. The flow was chosen to be steady-state for the same reasons mentioned in the two-dimensional model section.

3.4.1 Numerical Setup

ANSYS FLUENT can model the mixing and transport of chemical species by solving the conservation equations (24) . The species model was utilized for this simulation. Although the species transport model is traditionally used to solve problems with chemical reactions, it can be used to solve a species mixing model without reactions (24). The conservation equation takes the following general form:

$$\frac{\partial}{\partial t}(\rho Y_i) + \nabla.(\rho \vec{v} Y_i) = -\nabla.\vec{J_\iota} + R_i + S_i \text{ (ANSYS INC., 2017)}$$

In the previous equation, R is net rate of production of species i by chemical reaction and S_i is the rate of creation by addition from dispersed phase plus any user-defined sources (24). The same settings mentioned above were performed on the two and three-dimensional models.

In addition to species transport, ANSYS Fluent can model multiphase flow using the Volume of Fluid (VOF) method from the models. The VOF model simulates two or more fluids that don't dissolve in each other, also known as immiscible fluid (25). This is done by solving the momentum and continuity equations and tracking the volume fraction of each fluid in the domain (26). Although this modeling technique is used mostly to track a gas in a liquid or a liquid in a gas or a gas in a gas flow, literature of Du, Wei et. al shows it was used to track the volume fraction of a solid modeled as a fluid. The equation used for the conservation of mass, or what is also known as the continuity equation, can be expressed in the following form:

$$\frac{\partial p}{\partial t} + \nabla \cdot (\rho \vec{v}) = 0 \quad (26)$$

The equation used for the momentum conservation equation takes the following form:

$$\frac{\partial}{\partial t}(\rho\vec{v}) + \nabla \cdot (\rho\vec{v}\vec{v}) = -\nabla \mathrm{p} + \nabla \cdot (\bar{\bar{\tau}}) + \rho\vec{g} + \vec{F} \quad (26)$$

Where $(\bar{\bar{\tau}})$ is the stress tensor explained in the ANSYS Theory Guide.

The VOF model can be solved using the implicit or explicit formulation. The explicit is time dependent (26) so the implicit formulation was used here. The discretization of the implicit formulation can be found in the ANSYS Theory Guide which states:

$$\frac{\alpha_q^{n+1}\rho_q^{n+1} - \alpha_q^n \rho_q^n}{\Delta t} V + \sum_f \left(\rho_q^{n+1} U_f^{n+1} \alpha_{q,f}^{n+1}\right) = \left[S_{\alpha_q} + \sum_{p=1}^{n}\left(\dot{m}_{pq} - \dot{m}_{qp}\right)\right] V \quad (26)$$

Where n is previous time step, n+1 is the current time step, α is cell value of volume fraction, U is volume flux through the face and V is the cell volume (26).

The flow in both the two and three-dimensional models is laminar. The lubricant is very thin and in most practical cases the Reynolds number is low; therefore, the flow is laminar (27).

The same conclusion is reached to mathematically using the following equation:

$$Re = \frac{\rho * \omega * r * c}{\mu} \quad (27)$$

Where ρ is density of the fluid, μ is absolute viscosity, ω is rotational speed, r is radius of bearing and c is clearance. The resulting Re from solving that equation is 208. Therefore, the flow is laminar.

3.4.2 Solver Settings

The solver settings can greatly change the way ANSYS Fluent solves a model. Different schemes, under-relaxation factors and types of discretization render different results (24). The following settings were made to solve the two and three-dimensional original shoe models.

3.4.2.1 Two-Dimensional Model of the Original Shoe Model

The scheme chosen for solving the species transport model was SIMPLEC. The under –relaxation factor that can be applied to a SIMPLEC scheme is greater than that of SIMPLE scheme.

For the VOF model, a SIMPLE scheme was chosen as under-relaxation factors were not needed to be changed.

3.4.2.2 Three-Dimensional Model of the Original Shoe

Like the two-dimensional model, a SIMPLEC scheme was used for the species transport method and a SIMPLE scheme was used for the VOF method.

3.4.2.3 Three-Dimensional Model of the Shoe with the Injection Channel

For the species transport model, a SIMPLEC scheme was used, just like the two and three-dimensional models. On the other hand, the VOF model was solved using a SIMPLE scheme, also similar to the way the original shoe was modeled.

3.4.3 Spatial Discretization

The selection of an iterative scheme for discretizing the differential equations to solve the model is done by changing the selections of the spatial discretizations Fluent chooses as default. Gradient, pressure, momentum, species and volume fractions are each assigned a discretization method.

The gradient is a vector operator and is denoted by the symbol ∇. It used for directional derivatives (28). In the species model, the gradient discretization was assigned to be Green-Gauss Node Based. It calculates the gradient on the node instead of the default option, Green-Gauss Cell Based, which calculates the gradient on the center of the cell (24). The cell based calculations are less accurate but take less time to execute.

In the multiphase flow model using the VOF method, for the gradient, the Least Square Cell Based scheme was chosen.

In both the species and VOF models, the pressure term of the momentum equation was discretized using body force weighted scheme. For mixture or multiphase flow it is recommended in Fluent's user guide to use either PRESTO! (PREssure STaggering Option) or body force weighted scheme. PRESTO! is recommended for flows with high Rayleigh and swirl numbers (26). Since this flow contains no heat transfer, it would be wise to reduce computation time by excluding the energy equation and not choosing the PRESTO! scheme.

For the species model, a first order upwind scheme is used for the steel species and a second order upwind scheme is used for the water-oil mix species. First order upwind scheme is less aggressive than a second order upwind scheme. Convergence problems were faced running the species model, therefore, a first order scheme was chosen for the steel species. According the Fluent user guide, a first order scheme convergences easier but yields less accurate results than a second order scheme. It is acceptable though to use a first order scheme if the flow is aligned with a mesh (24). The mesh used here is orthogonal and the flow is normal to the boundary and therefore, a first order upwind scheme can be used without generating numerical error.

For the VOF model, a compressive volume fraction scheme was chosen. The compressive scheme is computationally less expensive than the other option available which is the modified HRIC (24).

Similar discretization schemes were applied to both of the three-dimensional models to solve the models using the same formulation and produce results that are discretely accurate.

For the spatial discretizations of the model of the shoe with the injection channel, Table 5 shows the settings selected for both species transport and VOF. To be consistent with the previous models of the original shoe, similar discretization methods were chosen.

Table 5 Discretization methods for the shoe model with the injection channel

	Species Transport	Volume of Fluid
Gradient	Green-Gauss Node Based	Least Squares Cell Based
Pressure	Body Force Weighted	Body Force Weighted
Momentum	Second Order Upwind	First Order Upwind
Water-oil mix	Second Order Upwind	N/A
Steel	First Order Upwind	N/A
Volume Fraction	N/A	Compressive

3.4.4 Under-Relaxation Factors

Under-relaxation factors are used to update the computations after each iteration according to the ANSYS Theory Guide (26). The under-relaxation factors were changed and tampered with to obtain a solution that converges and produce less computational error.

3.4.4.1 Two-Dimensional Model of the Original Shoe

The following table shows the values chosen for both the species and VOF methods for the two-dimensional model:

Table 6 under-relaxation factors for two-dimensional models of the original shoe model

	Species	VOF
Pressure	0.3	0.15
Density	1	0.5
Body Forces	1	0.5
Momentum	0.7	0.35
Steel Species	0.5	N/A
Water/oil mix species	0.5	N/A
Volume fraction	N/A	0.25

3.4.4.2 Three-Dimensional Model of the Original Shoe

The following table shows the values chosen for both the species and VOF methods for the three-dimensional model:

Table 7 under-relaxation factors for the three-dimensional models of the original shoe

	Species transport	VOF
Pressure	0.3	0.05
Density	1	0.25
Body Forces	1	0.25
Momentum	0.7	0.15
Steel Species	0.5	N/A
Water/oil mix species	0.5	N/A
Volume fraction	N/A	0.1

3.4.4.3 Three-Dimensional Model of the Shoe with the Injection Channel

The under relaxation factors used for both the species transport and VOF methods can be found in

Table 8 under-relaxation factors of the model of the shoe with fluid injection

	Species transport	VOF
Pressure	0.5	0.05
Density	1	0.25
Body Forces	1	0.25
Momentum	0.7	0.075
Steel Species	0.5	N/A
Water/oil mix species	0.5	N/A
Volume fraction	N/A	0.1

3.4.5 Monitors and Residuals

Residuals are a measure of convergence. The higher the residuals are, the greater the error. It is computed at each iteration. Generally, the lower this error is, the results have better chances of being correct (29). Lower convergence criteria does not necessarily mean the solution is inaccurate. Table 9 shows the convergence criteria chosen for all models of the original shoe and the shoe with the injection channel. It should be noted that for the two-dimensional models, the z-velocity is automatically eliminated from the residuals dialogue box.

Table 9 residuals for both the two and three-dimensional models of the original shoe

	Species	VOF
Continuity	1e-3	1e-3
x-velocity	1e-5	1e-5
y-velocity	1e-5	1e-5
z-velocity	1e-5	1e-5
Volume fraction water/oil	N/A	1e-5
Volume fraction steel	N/A	1e-5
Water/oil mix species	1e-5	N/A
Steel species	1e-5	N/A

3.5 Materials

The main reason species transport and VOF models were used is because of the presence of multiple materials. Multiple materials are mixing up in the simulation without any reactions or diffusions. The fluids flowing in the domain consist of three different materials. Table 10 includes all fluids used in the simulations and their properties. Small steel particles were modeled as a fluid because they flow in the fluid and are too small to disturb the flow.

Table 10 properties of materials used in the simulation (30)

	Density (kg/m^3)	Viscosity $(kg/m.s)$	Molecular Weight $(kg/kmol)$
Air	1.225	1.7894×10^{-5}	28.966
Coolant (94% water and 6% oil*)	998.2	0.001445	18.0152
Steel	8020	0.001445	55

* The oil used here is an industrial grade lubricant called Hocut™ model 796-RHS

In the transport species model for both the two and three-dimensional models, the mixture's density was calculated using volume weighted mixing law, the viscosity using mass weighted mixing law and mass diffusivity using constant dilute approximation.

3.6 Cell Zone Conditions

In the cell zone conditions second of Fluent there are two fluids. The fluid domain was split into two in ICEM CFD. The first one is the fluid under the shoe and the second one is the fluid everywhere else in the domain. This was done so that the fluid under the shoe can be patched and controlled to be the lubricant or in other words the water oil mix. This was done for all models, the two and three-dimensional ones.

3.7 Boundary Conditions

Each part created in ICEM must have a boundary condition assigned to it. The two and three-dimensional models have different boundary conditions. Even though in ICEM surfaces and edges can be assigned boundary conditions, the properties of those boundary conditions are determined in ANSYS Fluent.

3.7.1 Two-Dimensional Model

Even though the two2dimensional model has surface, boundary conditions were assigned to the curves bounding the model. Each boundary condition assigned to a curve can be seen in Figure 3-17.

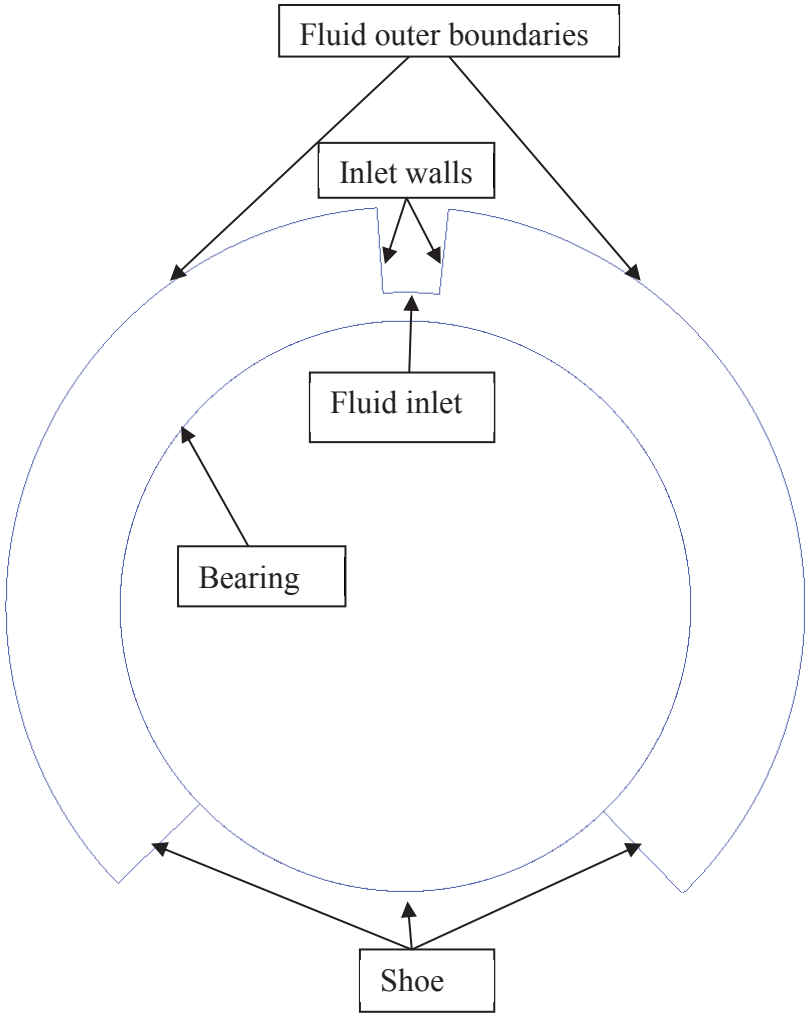

Figure 3-17 2D model boundary conditions locations

3.7.1.1 Fluid Inlet

The fluid inlet is where the mixture of water, emulsified oil and steel is injected as a mass flow rate. In their manufacturing process, bearings get machined from the top; in addition, water-oil mixture is supplied and sprayed constantly at a rate of 80 liters/min. Knowing the density of the water and oil mixture along with their volume fractions (96% water and 4% oil), the mass flow rate was calculated to be 1.35 kg/s. steel Particles from machining bearings had a ratio of 10 mg/100 ml of fluid. Therefore, as a mass fraction for the species transport model, water-oil mix was 0.99 and steel was 0.01 of the 1.35 kg/s

which is 0.0135 kg/s. For the multiphase flow, instead of mass fractions, volume fractions were assigned to the water oil mix and steel. Of the total volume, water oil mix was 0.99 of the volume fraction and the steel was 0.01. Air was assigned a 0 volume and mass fraction for both models.

3.7.1.2 Inlet walls

From Figure 3-17, the side walls labeled inlet walls were assigned as walls with no slip boundary conditions. These are the walls that bound our domain above the inlet edge.

3.7.1.3 Bearing

The boundary condition for the rotating bearing in Figure 3-17 is wall. It was set to be moving instead of stationary. Its movement was changed from translating to rotating. The axis of rotation is automatically set to the z-axis as this is a two-dimensional model. The rotation speed is set to 120 rad/s which translates to 1146 rpm. The bearing has a no slip shear condition.

3.7.1.4 Three Sides of the Shoe

All sides of the shoe, shown in Figure 3-17 were assigned to be stationary wall. With no slip boundary condition as well.

3.7.1.5 Pressure Outlets

The curves in Figure 3-17 that are labeled as pressure outlets were set to 0 pascal gauge pressure and zero backflow for the fluids.

3.7.2 Three-Dimensional Model

The three-dimensional model of the original shoe is more complex than the two-dimensional one. As far as geometry is concerned, it is merely an extrusion of the two-

dimensional model. Figure 3-18 and Figure 3-19 show the boundary conditions of the three-dimensional model of the original shoe.

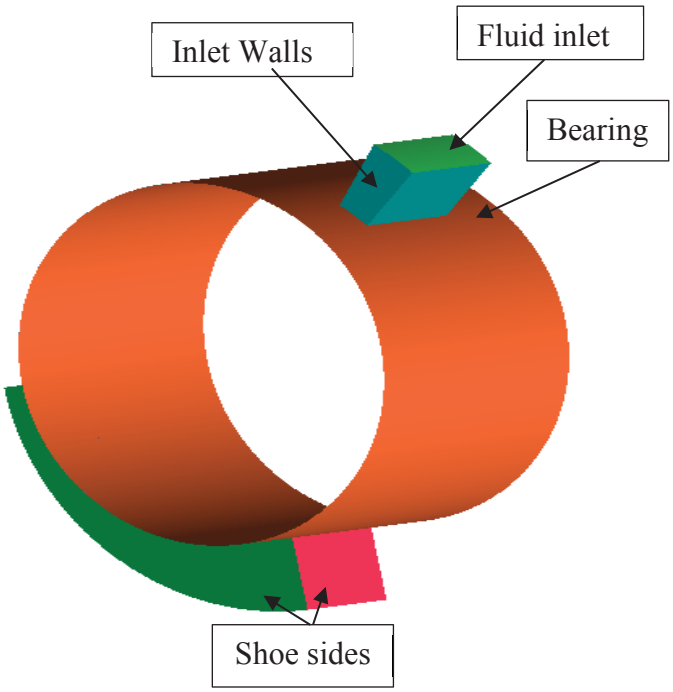

Figure 3-18 3D model boundary conditions

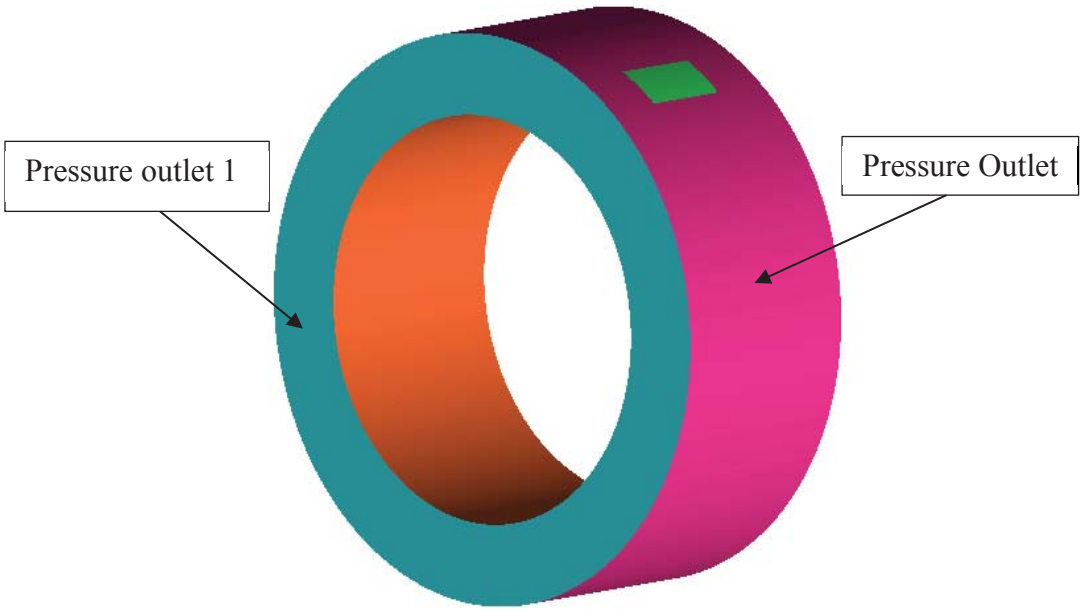

Figure 3-19 3D model, outlet boundary conditions

It is worth mentioning that for Figure 3-18, on the other side that is not shown there are two other walls that complete the sides of the shoe. There is also one more side for the shoe under the bearing. Furthermore, in Figure 3-19, the other side that is not shown has a pressure outlet identical to the outlet labeled pressure outlet 1.

3.7.2.1 Fluid Inlet

Like the two-dimensional model, the fluid inlet is where the mixture of water, emulsified oil and steel flows into the domain. Therefore, as a mass fraction, water-oil mix was 0.99 and steel was 0.01 of the 1.35 kg/s. As a volume fraction, for the multiphase model, the water/oil mix was assigned 0.99 of the 1.35 kg/s volume fraction and the steel was assigned 0.01 of that total volume.

3.7.2.2 Left, Right and Outer Boundaries

From Figure 3-19, all of the three boundaries were assigned to be pressure outlets. They had a gauge pressure of 0 pascal. None of the species or volume fractions flow back as they reach these boundaries.

3.7.2.3 Bearing

The boundary condition for the bearing in Figure 3-18 is a wall. It was set to be moving instead of stationary. Its movement was changed from translating to rotating. The axis of rotation is the z-axis. The rotation speed is 120 rad/s which translates to 1146 rpm. The bearing has a no slip shear condition.

3.7.2.4 Five Sides of the Shoe

All sides of the shoe, shown in Figure 3-18 were assigned to be stationary wall with no slip boundary condition.

3.7.2.5 Inlet walls

The walls around the inlet were assigned to be interior surfaces. They were shown for clarification purposes only.

3.7.3 Three-Dimensional Model of the shoe with the Injection Channel

The boundary conditions assigned to this model are very similar to those of the original shoe model. The only difference is the addition of the injection channel for the water/oil stream to be injected and deflect the steel particles. There are also small spaces on both sides of the shoe so that the water injected can flow out of the system. Figure 3-20 shows a general view of the model with the injection channel with the boundary conditions assigned to surfaces.

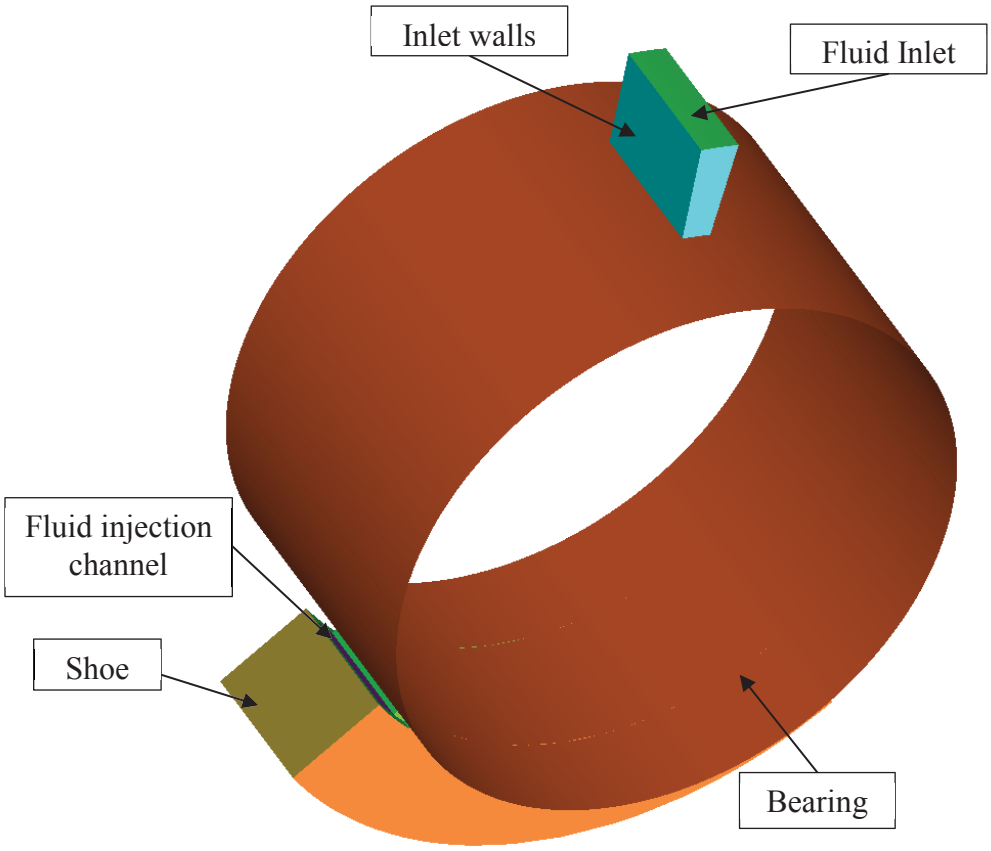

Figure 3-20 3D model with the injection channel, boundary conditions

3.7.3.1 Fluid Inlet

As stated previously, the fluid inlet is where the mixture of water, emulsified oil and steel flows in the system. A value for the mass flow rate boundary condition was set to be the same as the previous three-dimensional model of the original shoe.

3.7.3.2 Right, Left and Outer Pressure Outlets

Similar to the three-dimensional model of the original shoe model, the right. Left and outer sides of this model were set as pressure outlets. The gauge pressure was set to be 0 pascal. None of the species or volume fractions backflow into the model as they reach the boundary.

3.7.3.3 Bearing

The bearing was assigned a wall boundary condition. It was set to be a moving, rotational and no slip wall with a rotational speed of 120 rad/s. the axis of rotation is about the z-axis.

3.7.3.4 The Shoe

The shoe which is the embodied by the surface the bearing rests on and the four sides shown in Figure 3-20, were set to stationary walls with no slip boundary condition.

3.8 Initialization

A standard initialization was chosen for all models of the original shoe and the shoe with the injection channel. The initial values are shown in Table 11. It should be noted that for the two-dimensional models, the z-velocity is automatically eliminated from the residuals dialogue box.

Table 11 initialization values for the two and three-dimensional models

	Species	VOF
Gauge Pressure (pascal)	0	0
x-velocity (m/s)	0	0
y-velocity (m/s)	0	0
z-velocity (m/s)	0	0
Volume fraction water/oil	N/A	1
Volume fraction steel	N/A	0
Water/oil mix species	1	N/A
Steel species	0	N/A

As can be seen from

Table 11 the entire domain was initialized with water/oil mix. The reason behind that was that the coolant pump is always spraying water/oil mix to keep the process cool and not overheat.

Chapter 4 Results and Discussions

The results presented in this section are from the numerical and experimental investigation of the bearing manufacturing process. The experimental results include the static loading and wear test results. The numerical results include the outcomes from modeling the original shoe and modeling the shoe with the injection channel.

4.1 Experimental Results

The following subsections contain the results from the static loading test and the wear and aesthetics test.

4.1.1 Static Loading Test Results

The static loading test was done, using the Instron machine, to see how the shoes deflect under the normal grinding force of 150N. Shoes were also loaded to fracture and the data were recorded at 0.1 second intervals at a compression rate of 0.25 mm/min. Figure 4-1 and Figure 4-2 show the stress-strain curve for all shoes in addition to load vs deflection curves. The results showed that all of the shoes deflect less than 0.25 mm under 150N. Therefore, the results of these tests satisfied the required criteria. Figure 4-3 includes exact values of deflection under 150N load and the force value at which each shoe is deflected to 0.25 mm.

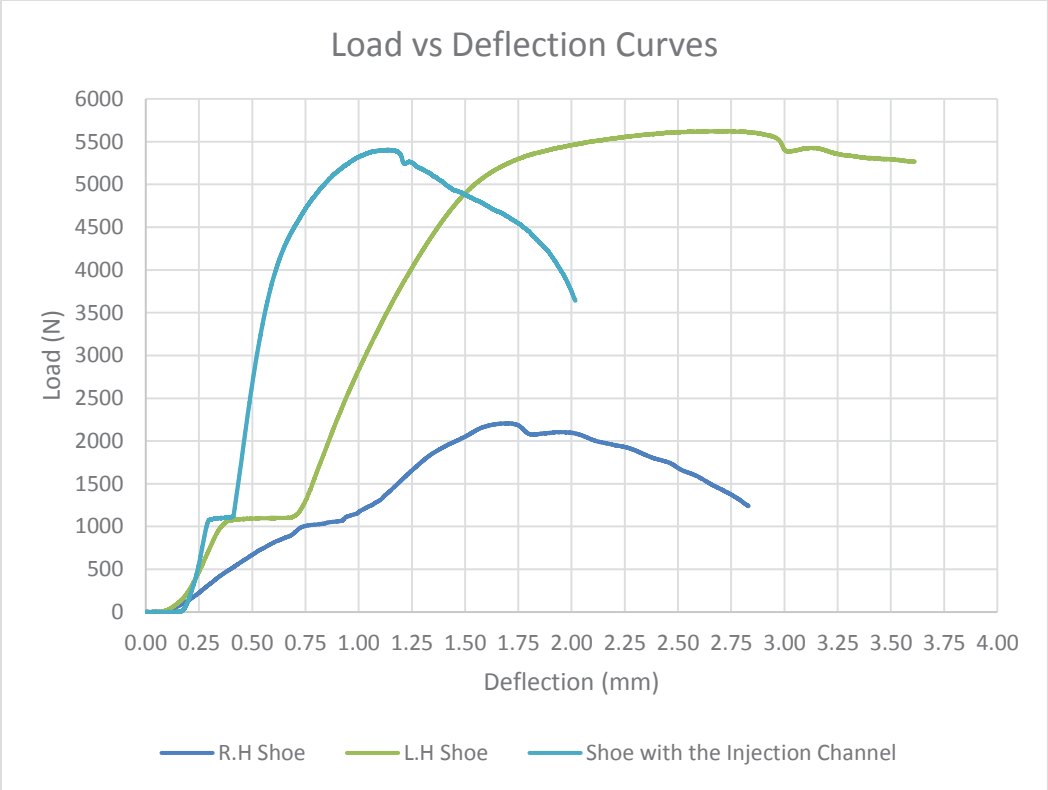

Figure 4-1 Load vs deflection

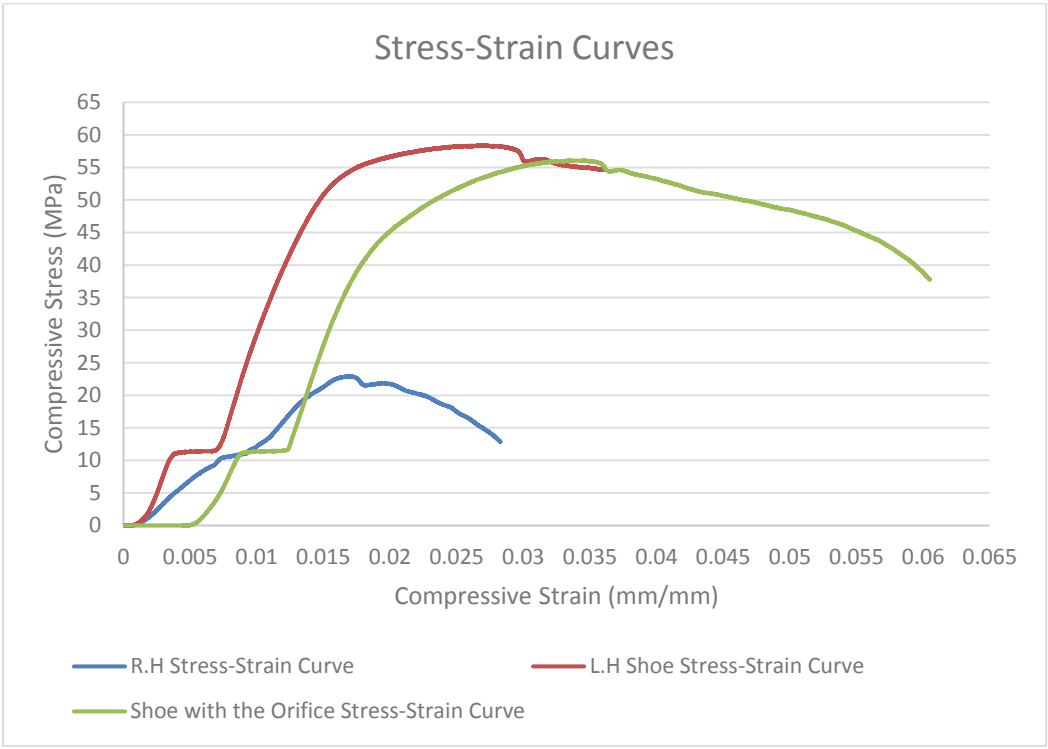

Figure 4-2 Stress-strain curves

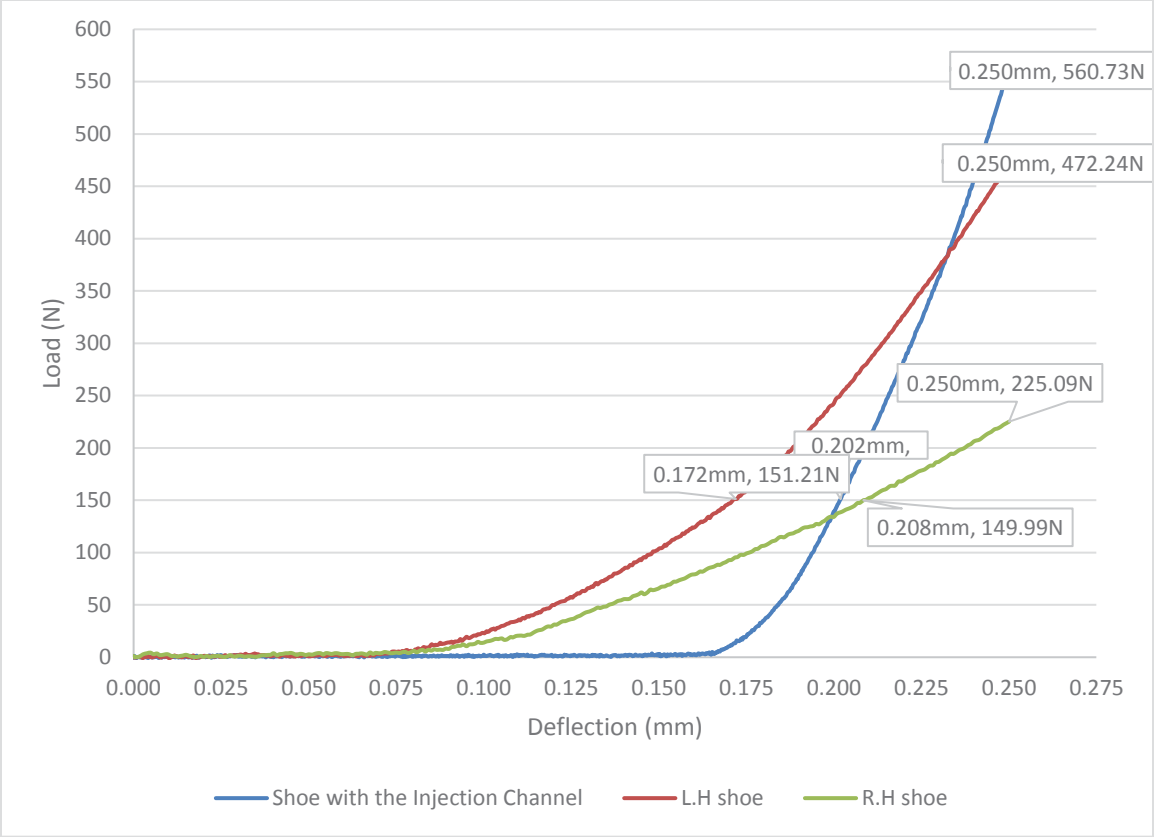

Figure 4-3 Maximum allowable deflection

4.1.2 Wear and Aesthetics Test

Three experiments were run using a lathe and the fixture designed to simulate the bearing machining process.

4.1.2.1 Dry Run Results

Both the right and left hand side shoes were weighed before and after running the test. The weight in grams for the shoes can be found in

Table 12 weight of shoes before and after testing

	Weight Before Testing (g)	Weight After Testing (g)	Wear Percentage (%)
R.H Shoe	2.3088	2.3171	-0.3582%
L.H Shoe	2.8578	2.8688	-0.3834%

The data in indicate that the shoes gained weight instead of losing due to the wear test. This could be explained by the contamination of the shoes with steel particles from the environment surrounding the lathe which usually contains small particles of steel. Contamination could have happened in the process of mounting the shoes and unmounting them. Moreover, the steel rod could have had residual steel particles from previous experiment. The residuals could also explain the increase in weight. To confirm, an untested new shoe was put under the microscope along with the shoe used for the dry run. The microscope used is Nikon SMZ800. The pictures were magnified 480 times.

From Figure 4-4, it can be seen that tiny steel particles are embedded in the shoe which could explain the gain in weight.

The shoe rubbing on the steel rod left black marks on the steel rod. This can be seen in Figure 4-5.

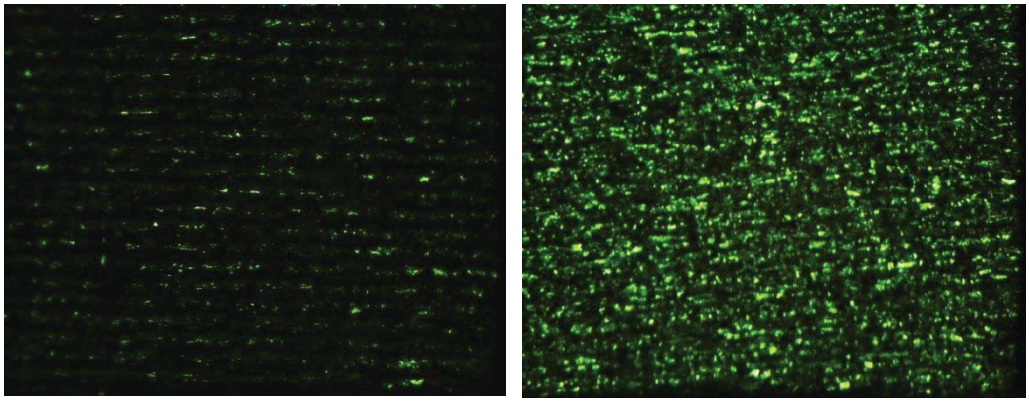

Figure 4-4 Dry run shoe surface before (left) and after (right)

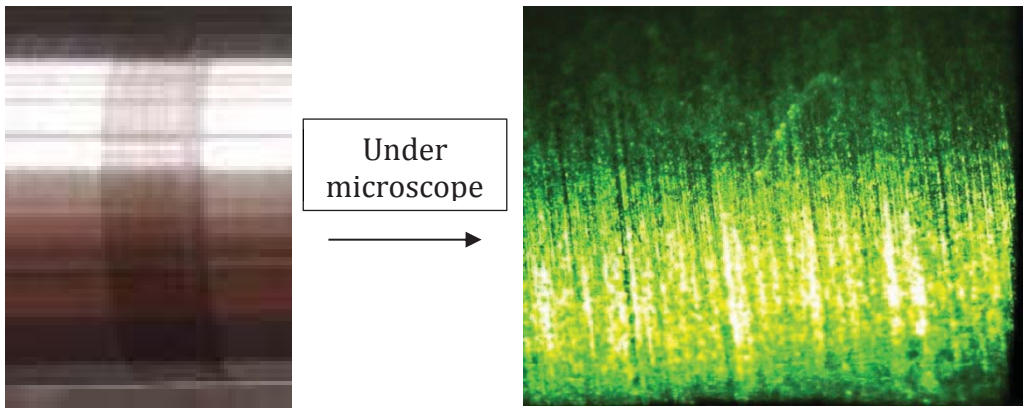

Figure 4-5 Shining band, dry run

4.1.2.2 Clean Wet Run

This run was performed to see the effect of running the shoes with lubricant only. The shoe was put under the microscope to see the effect the wet clean run against the rod had on it. The microscopic picture is captured in Figure 4-6 on the left and compared to a clean new shoe on the right.

The surface of the shoe sustained less damage than the dry run because of the lubricant. Also no clear sight of steel particles can be found on the image under the microscope. The shoe left a mark on the steel rod. The change in the steel rod can be seen in Figure 4-7.

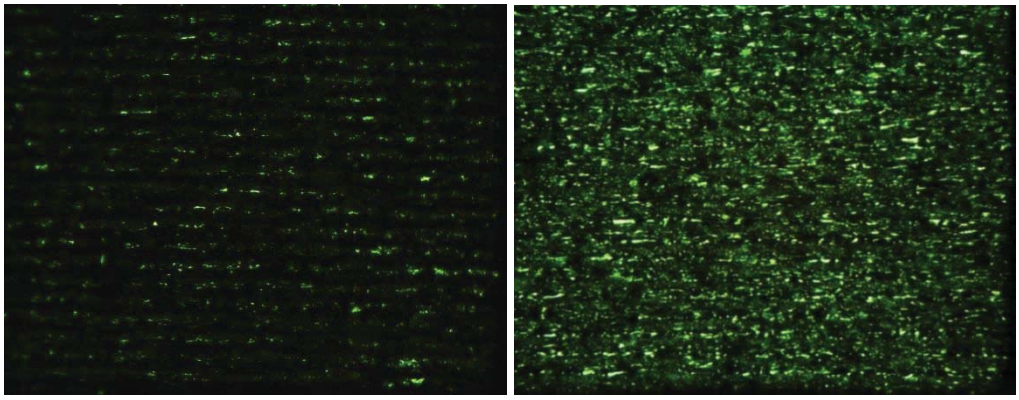

Figure 4-6 Clean wet run shoe surface before (left and after (right)

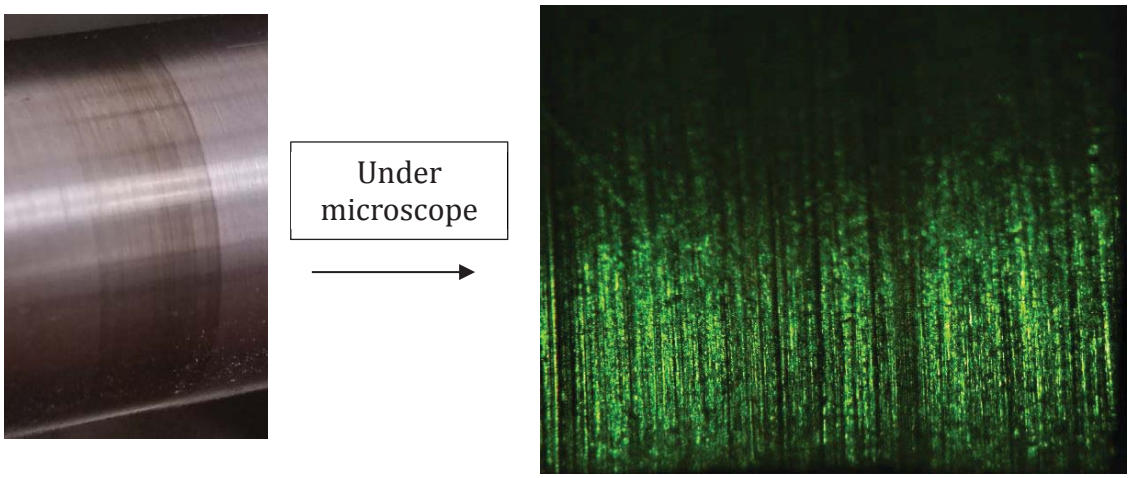

Figure 4-7 shining band, clean wet run

The shining band on Figure 4-7 are caused by the friction between the shoe and the steel rod

4.1.2.3 Dirty Wet Run

Particles were injected during the run to simulate the particles flying from the bearing machining process. The shoes sustained more damage than the clean wet run and the steel rod was left with a more defined mark than the clean wet run. Figure 4-8 and Figure 4-9 show the result of the experiment on the shoe and steel rod section used in this run

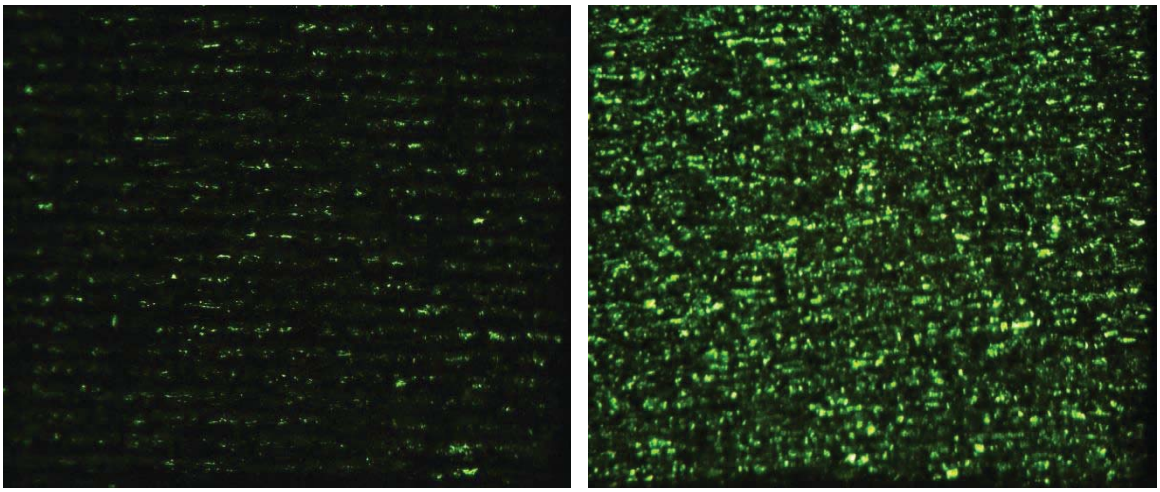

Figure 4-8 Dirty wet run shoe surface before (left and after (right)

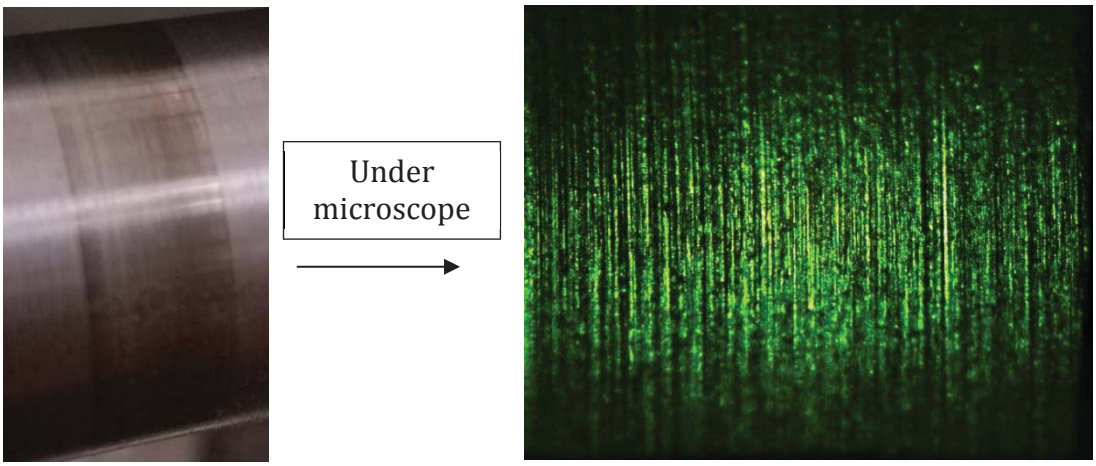

Figure 4-9 Shining band, dirty wet run

The steel rod used for the dry, clean wet and dirty wet runs can be seen in Figure 4-10. The stripe on the far right is the darkest and is the result of the dry run. The middle stripe is a shade darker and it is the result of the dirty wet run. The clean area in the middle of that stripe is from the injection channel and the darker areas are from the shoe rubbing against the steel. The stripe on the far left has the lightest shade and it is the result of the clean wet run. Also, the effect of the injection channel can be seen in the right half of the steel rod. The part where the experiment was performed was sanded and cleaned so that little scuffs and blemishes don't affect the outcome of the experiment.

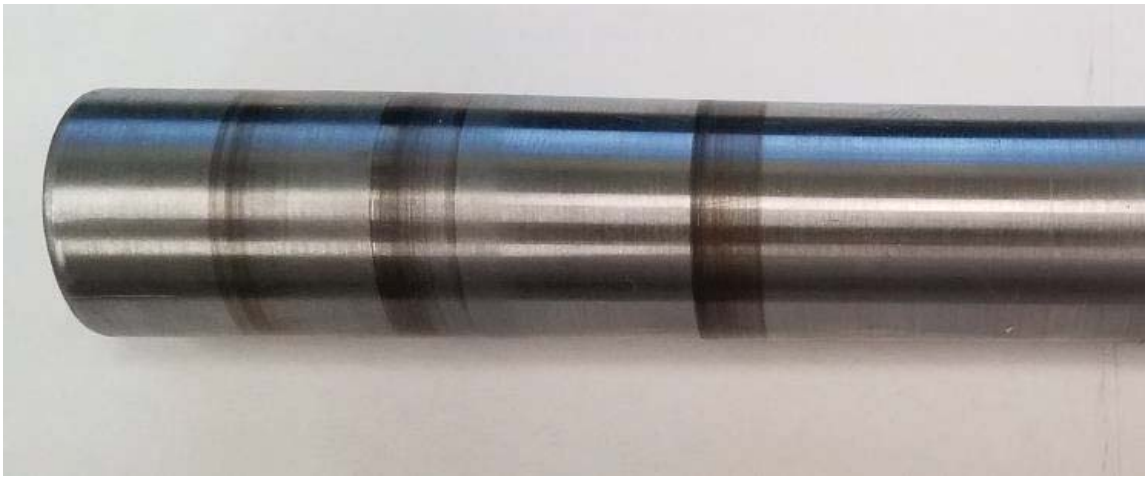

Figure 4-10 Steel rod used for testing.

4.2 Numerical Results

4.2.1 Two-Dimensional Model of the Original Shoe Results

4.2.1.1 Species Transport Model Results

The two-dimensional model for the species transport was run for a total 825,000 iterations. It was observed that the model reached a steady state at that point. Figure 4-11 shows the steel species along with a zoomed in view of the area between the bearing and the shoe where the shining band problem occurs. From Figure 4-11, the steel species go in to about one fourth of the curve of the shoe and that is enough to cause scratches on the bearing rotating on it.

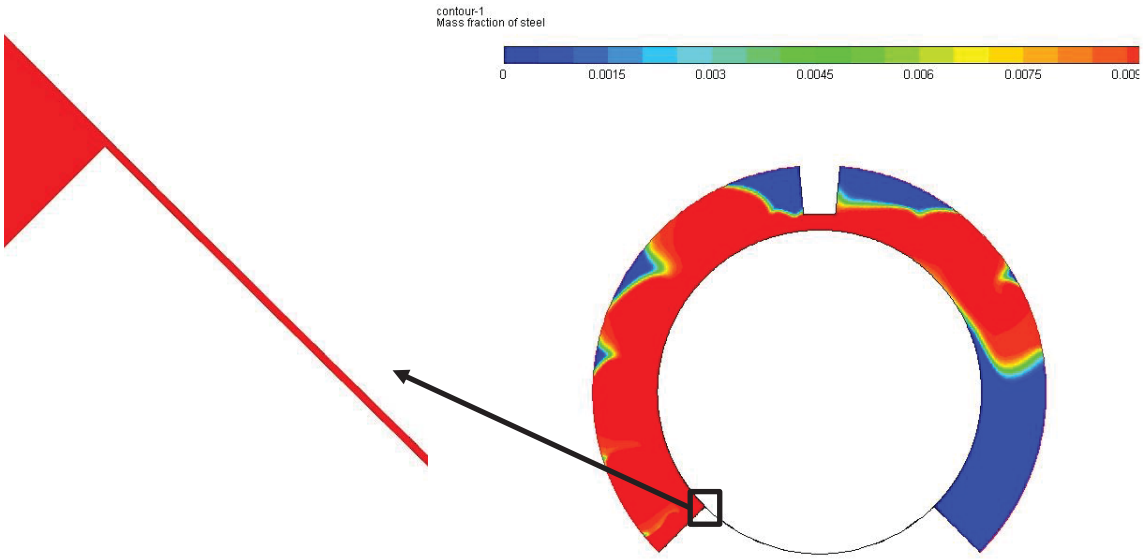

Figure 4-11 Steel mass fraction of the two-dimensional model of the original shoe

In addition, Figure 4-12 show the water/oil mix mass fractions in the fluid domain around the bearing and in between the gap between the shoe and the bearing. This result is expected as the bigger mass fraction of the fluid (0.99) is the water/oil mix. As a result, the red shade of the water/oil mix contour shows a mass fraction of 0.99. Figure 4-13

shows velocity vectors of the fluid in the critical region of the fluid domain. A velocity profile containing both Poiseuille and Couette is forming. The Poiseuille profile forms in the presence of a pressure increase. Since the fluid heads to flow in a smaller region as it approaches the gap between the bearing the shoe, a Poiseuille profile forms. The Couette profile forms in the presence of viscous forces. Since the fluid is reaching the wall of the shoe, the Couette profile forms. The velocity at the shoe which is a wall is zero.

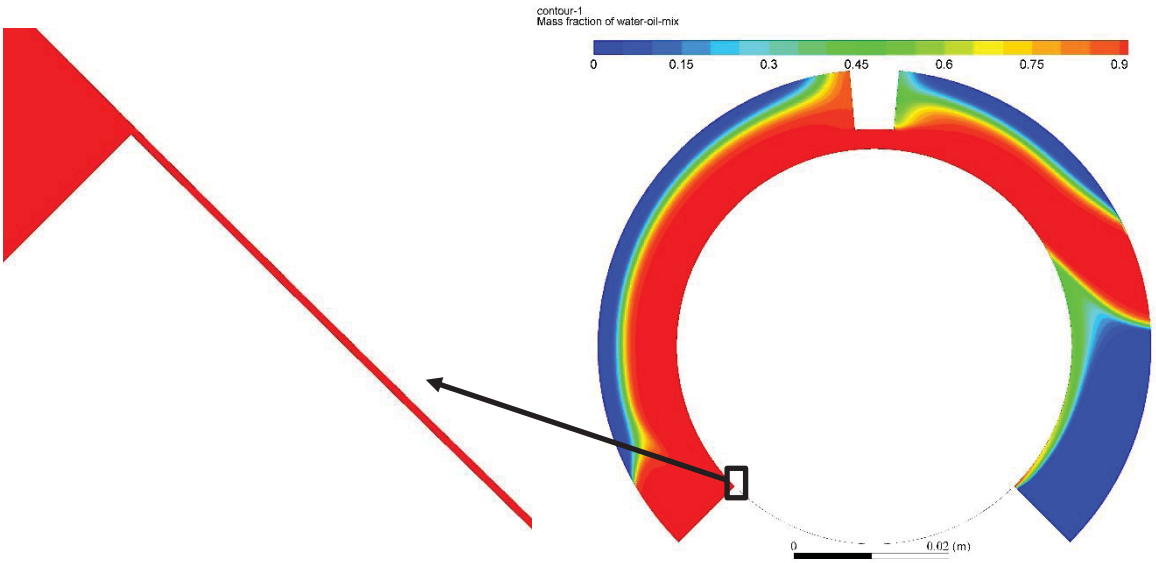

Figure 4-12 Water/oil mass fraction of the two-dimensional model of the original shoe

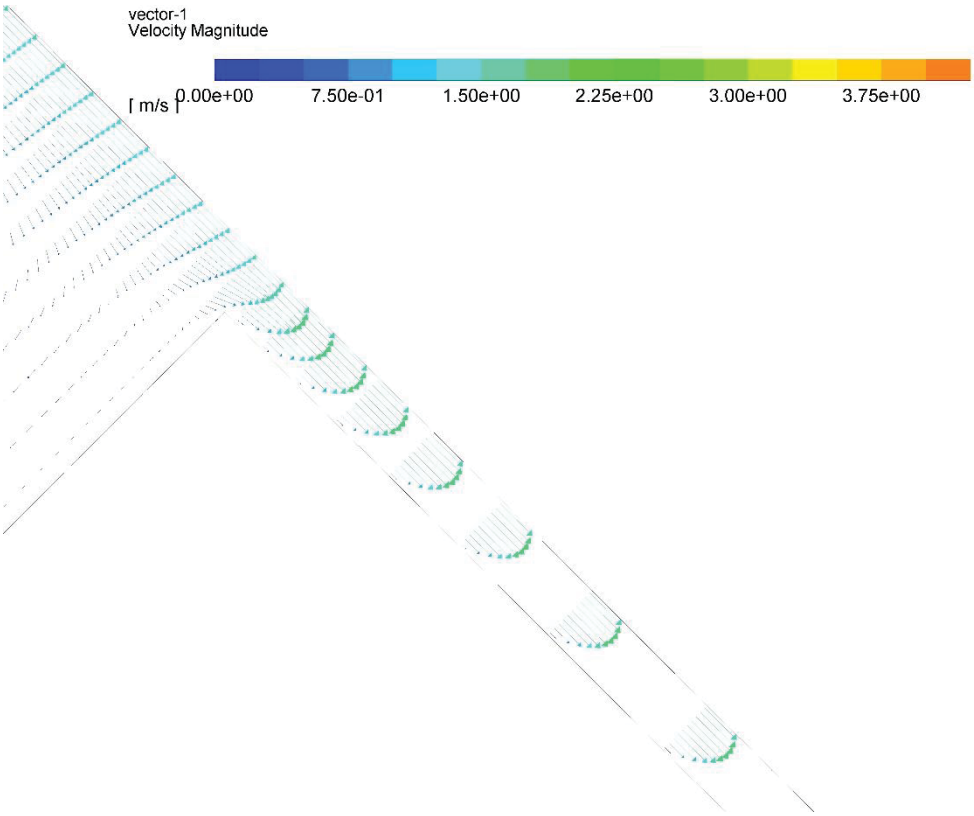

Figure 4-13 Velocity vectors of two-dimensional species transport model of the original shoe

The amount of steel, water-oil mix and air species going through the gap between the bearing and the shoe is computed by Fluent using an area weighted average method. The results can be found in Table 13.

Table 13 Species mass fractions for the two-dimensional model

	Mass fraction
Steel species	0.0099846595
Water-oil mix species	0.98848131
Air species	0.0015340707

4.2.1.2 Volume of Fluid Model Results

Although the formulation of the VOF method is different from the species transport's formulation, the results are similar. A concentration of steel fraction is apparent on the

first quarter of the curve of the shoe. The way it is expressed in the following figures different. While transport species shows contours as mass fractions, VOF shows contours as volume fractions. The volume of fractions of steel can be seen in Figure 4-14. The scale used for displaying the steel volume fractions is different from that of the mass fraction.

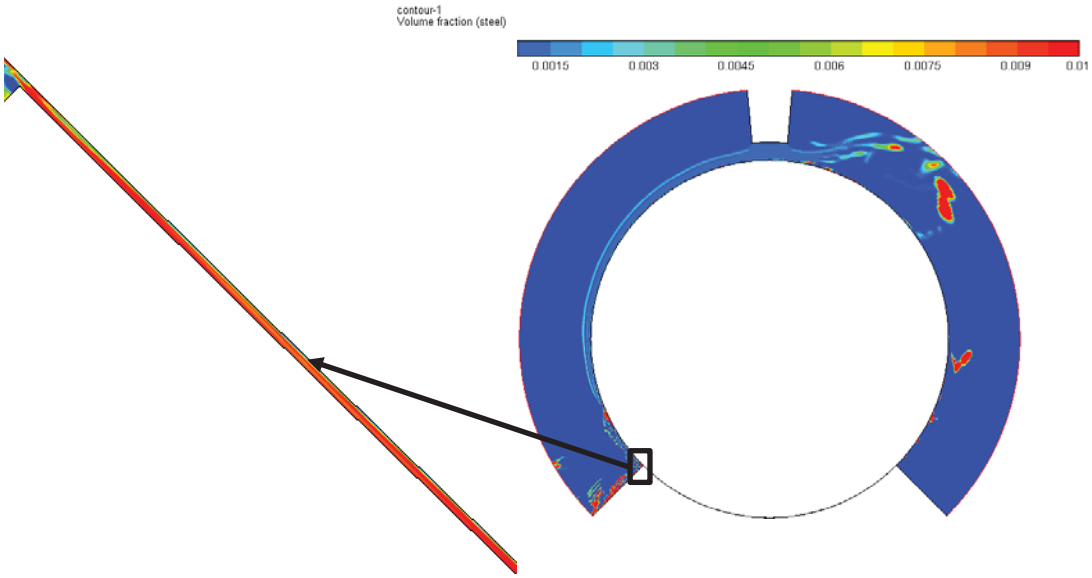

Figure 4-14 Steel volume fraction of the two-dimensional model of the original shoe

The small drops separating from the steel boundary layer around the bearing are steel concentrations. While that is not the case with the species transport model. This can be explained by the fact that the multiphase flow different separate fluids while the species transport uses a mixture of fluid. So in the species transport case, all the fluids are uniformly mixed which creates a homogeneous mixture. The volume of fluid method is different. It treats fluids differently. Nevertheless, the steel volume fraction still concentrates in the first quarter of the area between the shoe and bearing.

In Figure 4-15 the water/oil mix volume fractions are shown. As water pours from the inlet and reaches the rotating bearing, the water takes the shape of the counterclockwise

rotation. A zoomed in picture of the gap between the shoe and the bearing is also shown where the water/oil mix enters that small domain as expected to happen. Figure 4-16 shows velocity vectors of the fluid in the critical region between the shoe and the bearing. The vectors are all the same length because of the difference in velocity gradient which shows the arrows growing exponentially and the results from that are not clear.

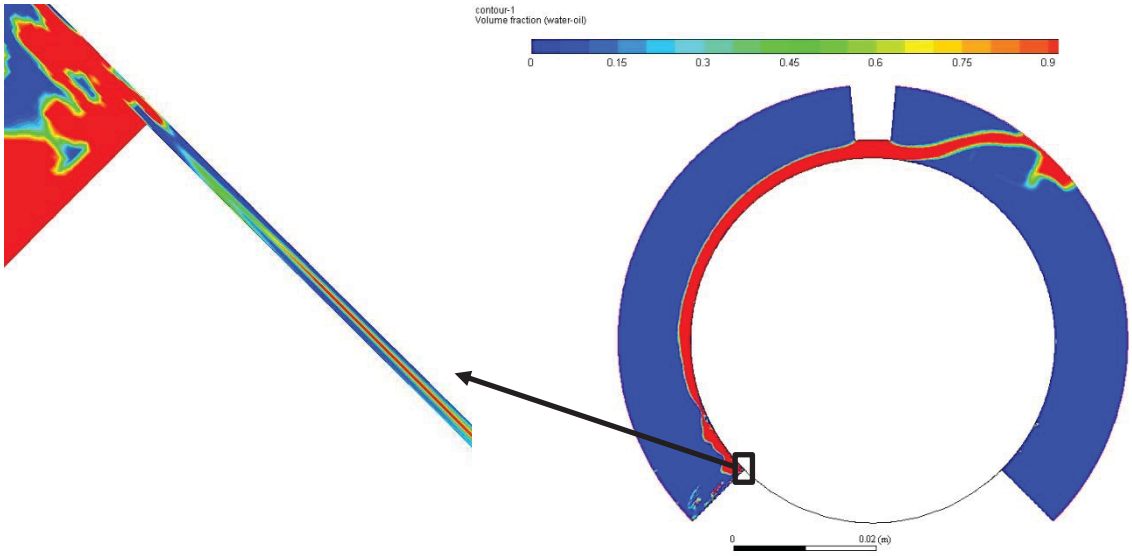

Figure 4-15 Water/oil volume fractions of the two-dimensional model of the original shoe

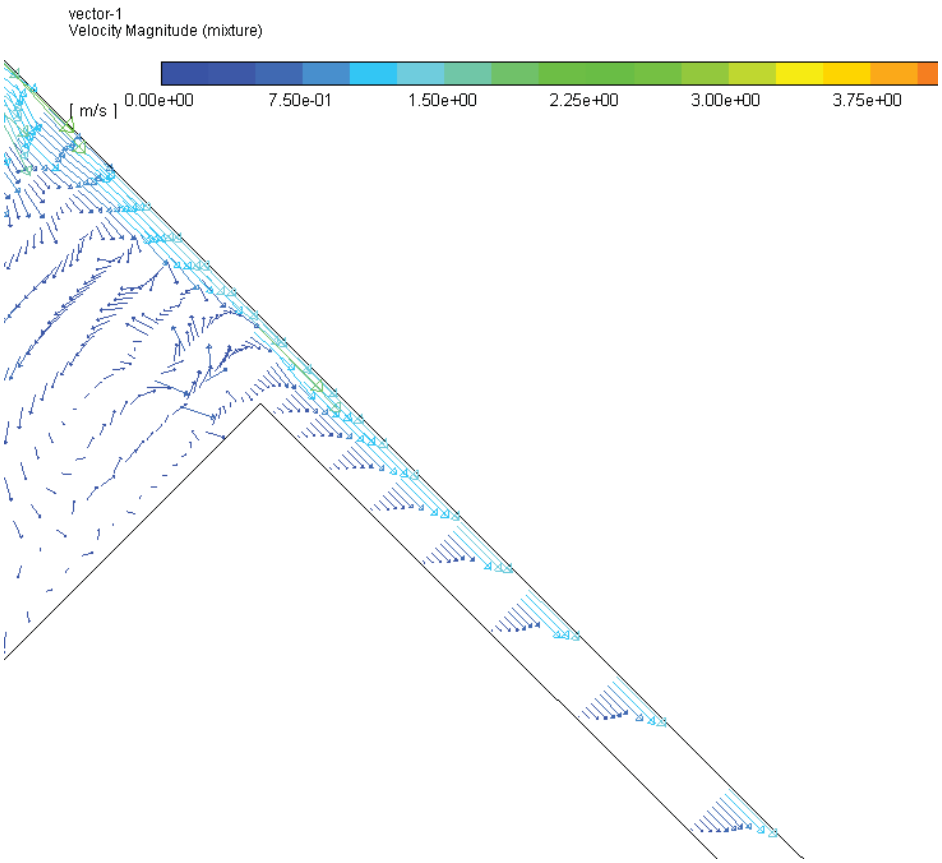

Figure 4-16 Velocity vectors of the two-dimensional volume of fluid model of the original shoe

Table 14 includes the volume fractions of each fluid going in the gap between the bearing and the shoe.

Table 14 volume fractions of the two-dimensional model

	Volume fraction
Steel volume fraction	0.6245369
Water-oil mix volume fraction	0.033344709
Air volume fraction	0.34211843

4.2.2 Three-Dimensional Model of the Original Shoe Results

Similar to the two-dimensional model, the three-dimensional model was run using both the species transport and volume of fluids methods. The results will be presented in the next subsection.

4.2.2.1 Species Transport Model Results

The three-dimensional model of the original shoe was run for a total number of 350,000 iterations. The simulation was stopped every 50,000 iterations to check if steady state was reached. Since the residuals did not reach the convergence criteria, the simulation had to be stopped at the convergence point which was determined by the amount of change in the model every 50,000 iterations. Figure 4-17 shows the steel transport species.

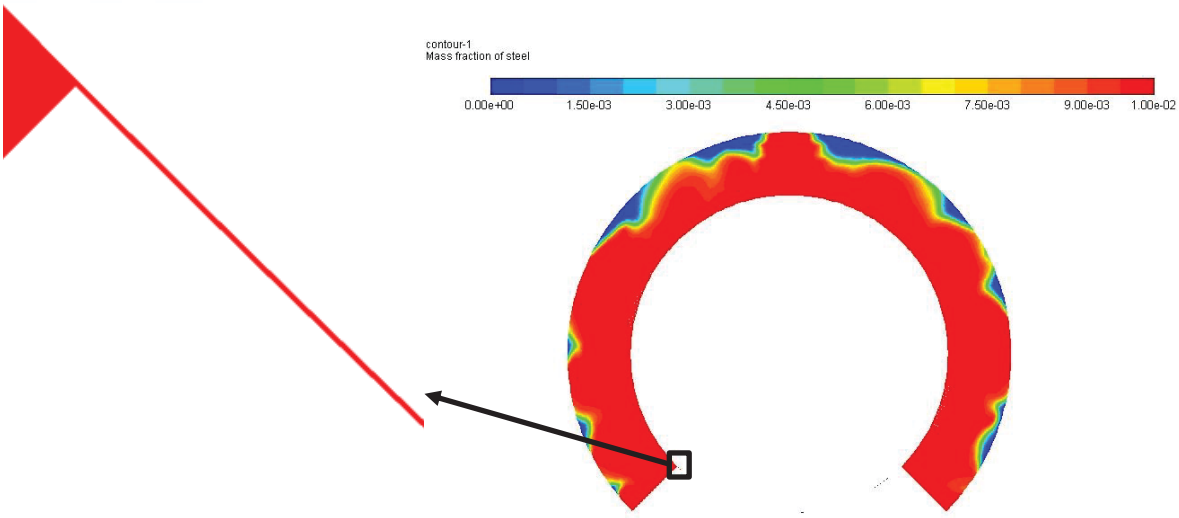

Figure 4-17 Steel mass fractions of the three-dimensional model of the original shoe

As can be seen from Figure 4-17, the results of the center plane cut of the three-dimensional model is very similar to the plane contour of the two-dimensional model. In addition, water/oil mix contour takes a similar path to that of the steel mass fraction contour. The contour for water/oil mix mass fraction can be seen in Figure 4-18. The velocity vectors in the same region can be seen in Figure 4-19. The velocity is maximum where the bearing rotates and zero near the wall of the shoe which is stationary.

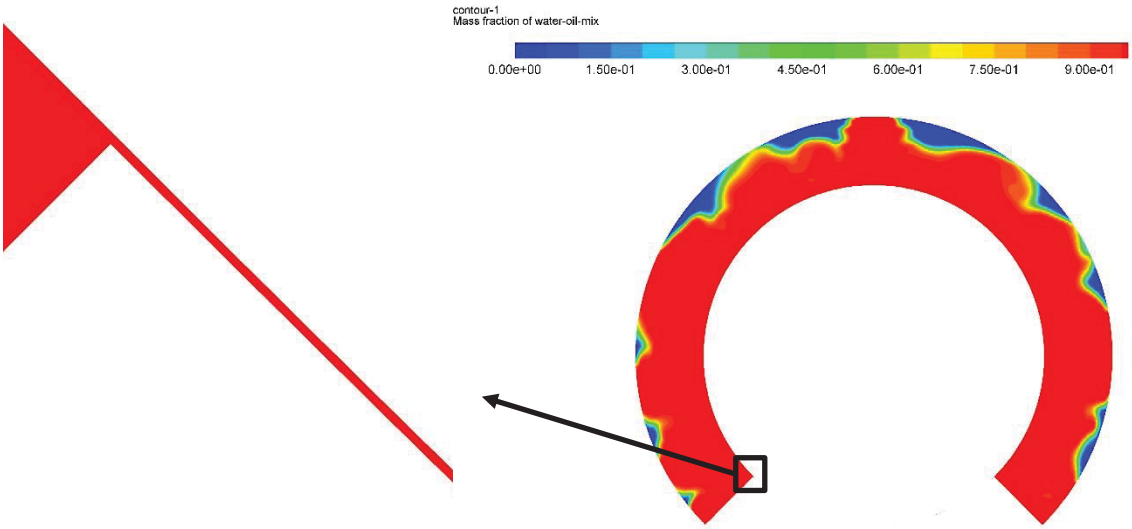

Figure 4-18 Water/oil mass fraction of the three-dimensional model of the original shoe

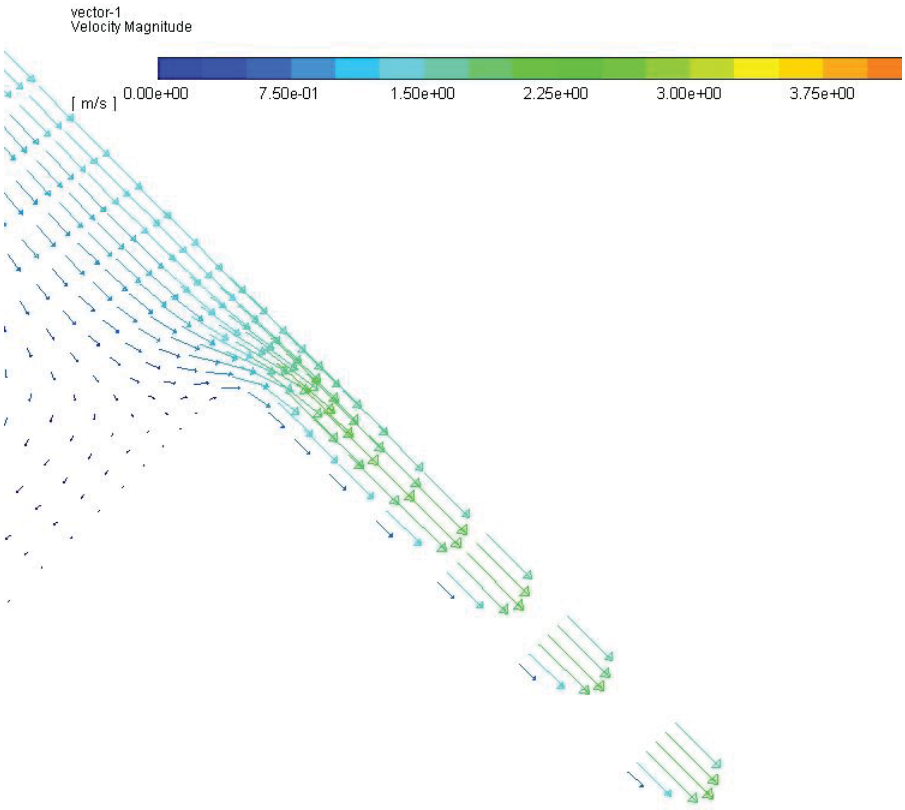

Figure 4-19 Velocity vectors of three-dimensional species transport model of the original shoe

Table 15 shows the mass fractions between the bearing and shoe.

Table 15 Mass fractions of the three-dimensional model

	Mass fraction
Steel species	0.0098032555
Water-oil mix species	0.98530902
Air species	0.0048454143

4.2.2.2 Volume of Fluids Model Results

Volume fraction results from running the three-dimensional model of the original shoe model are shown in this section. Figure 4-20 shows the steel volume fraction contour. This result corresponds to what was originally obtained in from the two-dimensional model of the original shoe. The flow of steel around the right half of the bearing is not exactly the same. That can be explained by the variation of geometry in the three-dimensional model, however the rest of the flow follows a similar path of that of the two-dimensional model. .

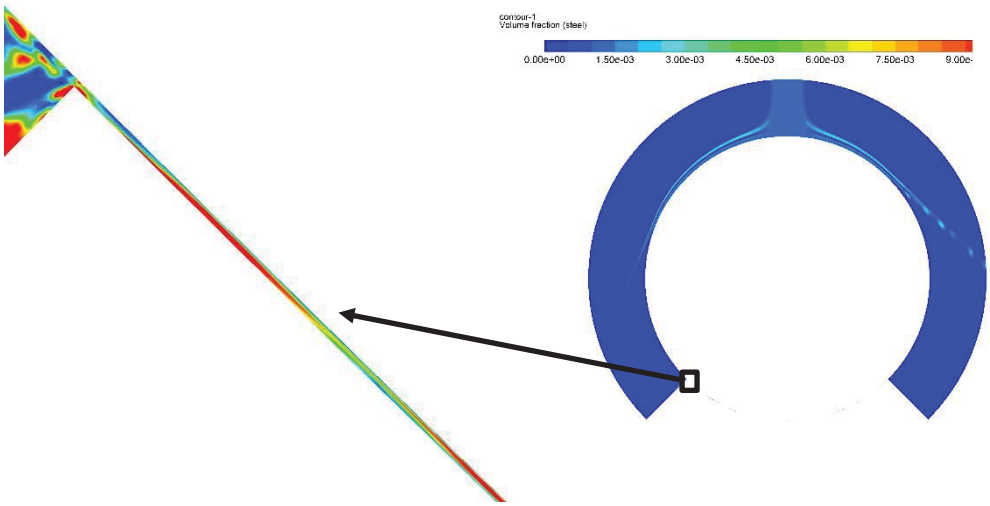

Figure 4-20 Steel volume fraction of the three-dimensional model of the original shoe

In Addition, the water/oil mix volume fraction of the three-dimensional model of the original shoe shows contours similar to the steel fractions but with bigger volume fraction. This result is natural because of the assigned volume fraction of water/oil is 0.99 and steel is 0.1 so it expected to see darker more red contours in the same regions. The

velocity vectors of this model are shown in Figure 4-22. Since the vectors shown are of fixed length, a zoomed in view of the original length with the right arrow lengths is also shown. In addition, Table 16 shows the steel, water and air volume fractions at the entrance of the gap between the shoe and bearing.

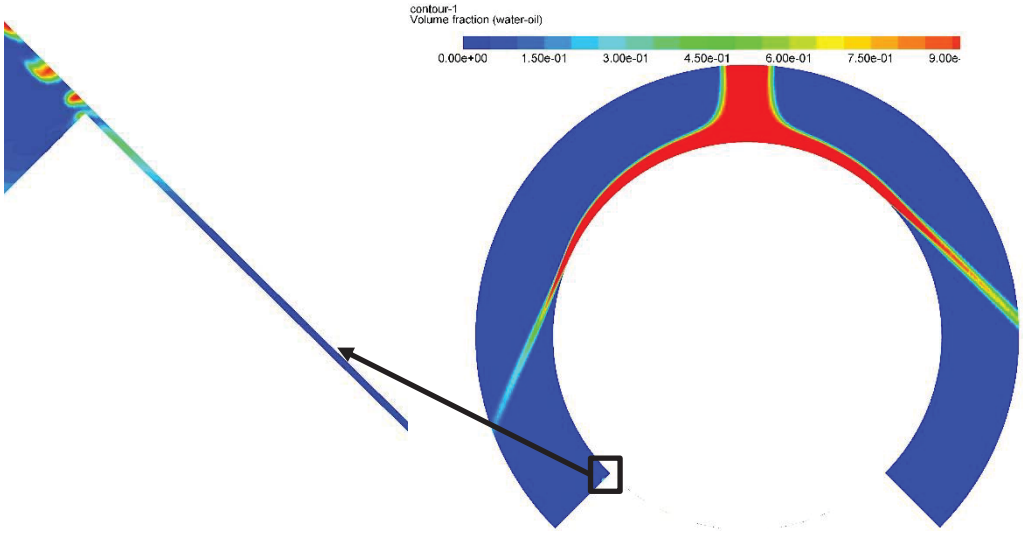

Figure 4-21 Water/oil volume fraction of the three-dimensional model of the original shoe

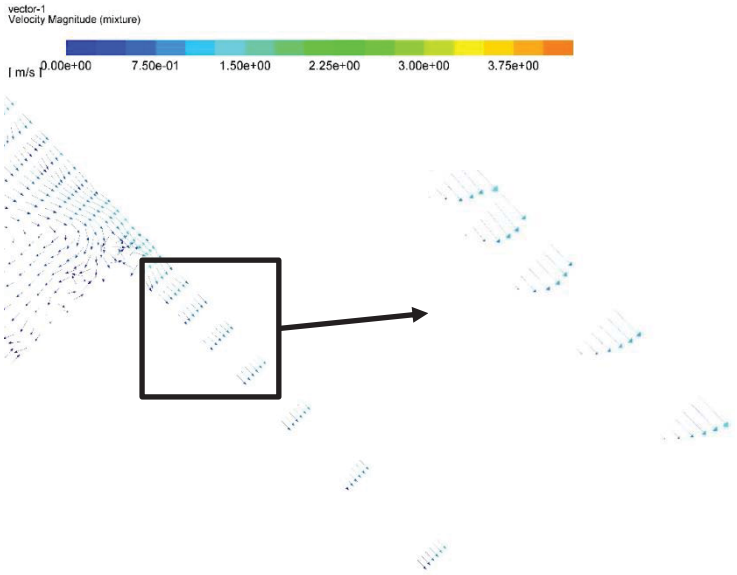

Figure 4-22 Velocity vectors of the three-dimensional volume of fluid model of the original shoe

Table 16 Volume fractions of three-dimensional model of the original shoe

	Volume fraction
Steel volume fraction	0.1495644
Water-oil mix volume fraction	0.2353337
Air volume fraction	0.6150495

4.2.3 Shoe with the Injection Channel Model Results

Species mass fractions and multiphase flow volume fractions results from running the model with the shoe with the injection channel are presented in the next subsection.

4.2.3.1 Species Transport Results

The result from running the model of the shoe with the injection channel reduced the amount of steel species transport significantly. Figure 4-23 shows the contour for steel species mass fraction.

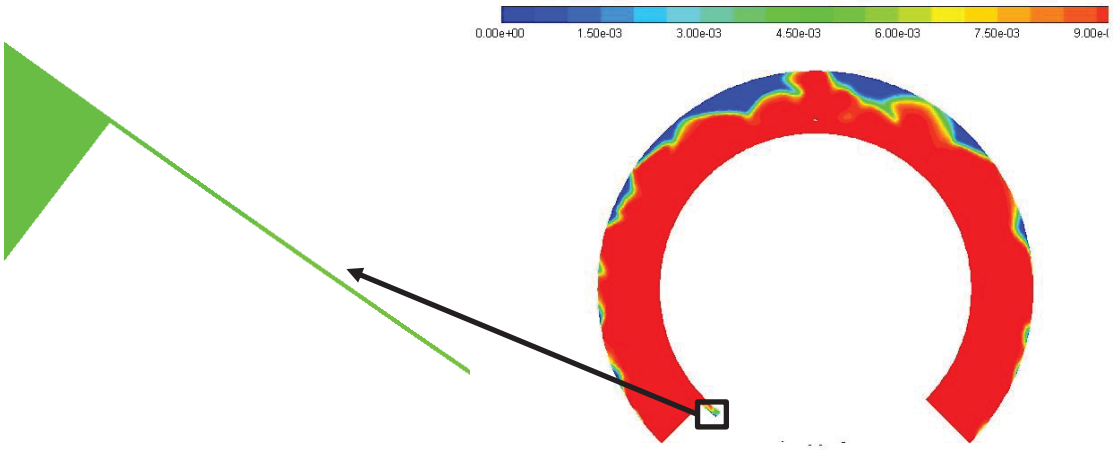

Figure 4-23 Center plane cut of the model with the injection channel steel mass fractions

In addition, water/oil mix mass fractions show a similar flow profile around the bearing and in the small gap in between the shoe and the bearing to that of the steel mass fractions of the shoe with the injection channel model. The water/oil mix contours can be seen in Figure 4-24. In Figure 4-25, velocity vectors can be seen with a velocity profile similar to what to be expected in that region. The velocity near the wall goes to zero and

it maxes out near the bearing. Also Table 17 shows the mass fractions of air, water/oil and steel at the entrance of the gap between the shoe and bearing. It also compares the percentage of mass fractions from the model of the original shoe to the model with fluid injection channel. A huge part of the steel species was deflected which proves that this model works for the intended purpose it was created for.

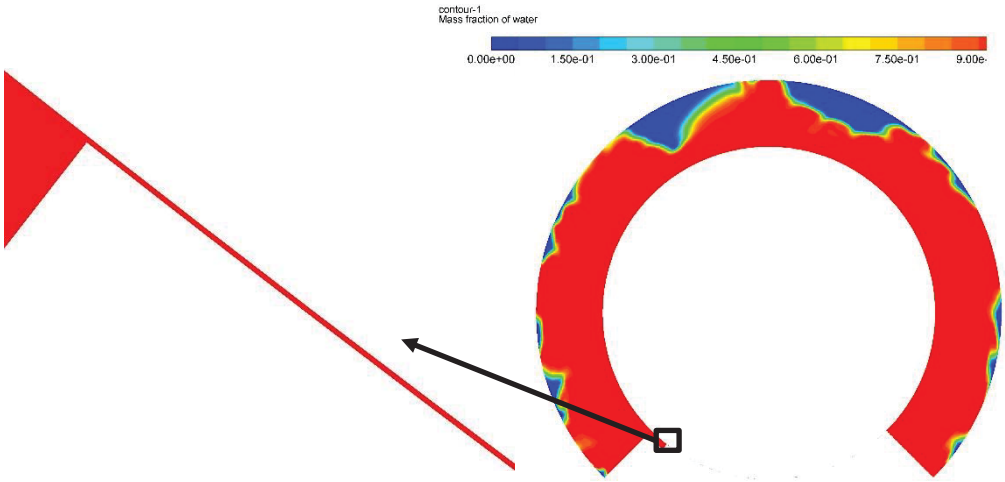

Figure 4-24 Water/oil mass fractions of the shoe with the injection channel model

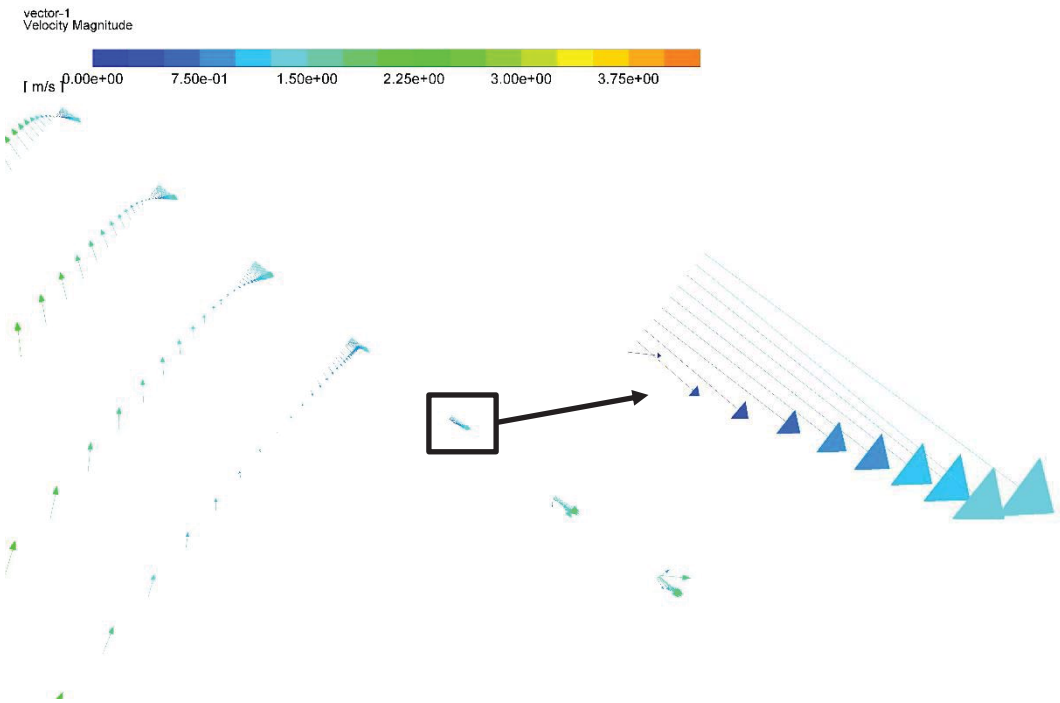

Figure 4-25 Velocity vectors of the shoe with the injection channel species transport model

Table 17 Mass fractions of species of the shoe with the injection channel model

	Mass fraction	Percentage difference
Steel species	0.0022315461	-77.24%
Water-oil mix species	0.9967952	1.15%
Air species	0.0009190939	-81%

4.2.3.2 Volume of Fluids Results

Running the model of the shoe with the injection channel reduced the amount of steel volume fractions significantly. Figure 4-26 shows the contour for steel volume fraction.

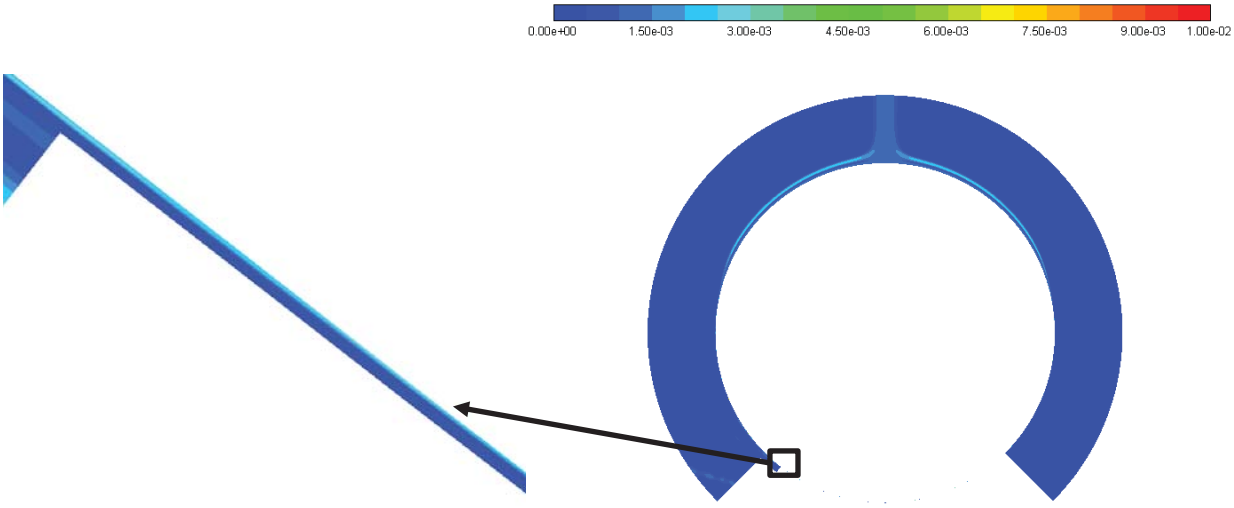

Figure 4-26 steel volume fractions of the shoe with injection channel

In addition, water/oil mix volume fractions, in Figure 4-27, show a similar flow profile around the bearing and in the small gap in between the shoe and the bearing to that of the steel volume fractions of the shoe with the injection channel model. The water/oil mix contours can be seen in. In Figure 4-28 the velocity vectors can be seen with a profile matching what is expected to happen. The velocity is maximum near the bearing and approaches zero as the profile comes closer to the wall of the shoe. Also

Table 18 shows the volume fractions of air, water/oil and steel at the entrance of the gap between the shoe and bearing. It also compares the percentage of volume fractions from the model of the original shoe to the model with fluid injection channel

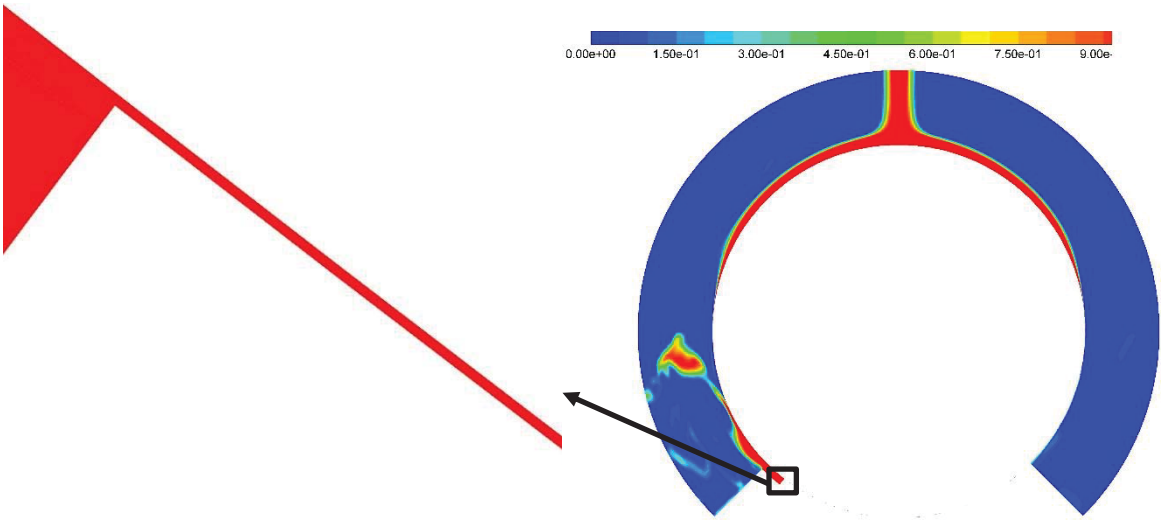

Figure 4-27 water/oil volume fractions of the shoe with the injection channel

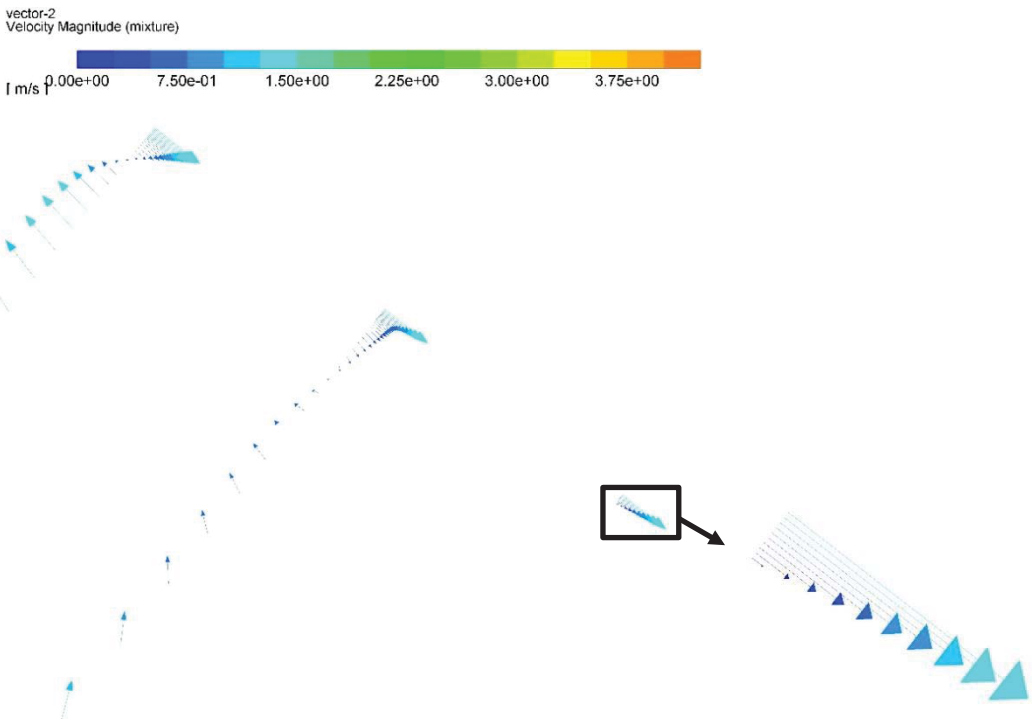

Figure 4-28 velocity vectors of the shoe with the injection channel volume of fluid model

Table 18 volume fractions of the VOF model of the shoe with injection channel

	Volume fraction	Percentage difference
Steel volume fraction	0.00084518573	-99.43%
Water-oil mix volume fraction	0.9988006	76.43%
Air volume fraction	0.0003000276	-99.95%

In Table 19, all of the mass and volume fractions steel were converted to grams/s at the entrance of the gap between the bearing and shoe to compare all two and three-dimensional models of the species transport and volume of fluids methods.

Table 19 all volume and mass fractions of steel converted to grams/s flow rate

	Two-dimensional		Three-Dimensional		Three-Dimensional Injection Channel	
	Species Transport	VOF	Species Transport	VOF	Species Transport	VOF
Steel (fraction)	0.009985	0.6245	0.0098	0.1496	0.002287	0.000845
Steel(g/s)	0.0161	4.23	0.0052	0.0124	1.8e-5 g	6.33e-5

Chapter 5 Conclusion and Future Work

5.1 Conclusion

5.1.1 Experimental Conclusion

The shining band phenomenon was not eliminated from the outer surface of the steel rod. However, that shining band could be attributed to a reason other than steel particles rubbing against the steel rod as it rotates. It could be the material of the shoes rubbing on the steel rod. Since the material of the shoes is carbon fiber filament, its color is black and the shining band on the steel rod has a darker shade than the shade of steel, it leads to the conclusion that the shining was not caused by the steel particles but rather by the shoes themselves.

The main conclusion obtained from the static loading test is that all shoes, the left, right and shoe with injection channel can withstand a static loading of 150N with deflection less than 0.25 mm. this result is important because any additional deflection would affect the machining process and may lead to fault dimensions.

The second experiment was the wear rate and aesthetics test. Since the shoes were contaminated and the weight increased instead of the expected result which was decrease in weight, the only conclusion that could be drawn is that after half an hour of dry rubbing against the steel rod, the shoes did not wear significantly. The contamination particles are small and cannot be seen with naked eye, therefore, the weight gain from particles is insignificant. This also means that the weight loss from friction is insignificant too.

The original belief that the shining band is caused by steel particles was negated with the observation that the shining band still occurred after running only clean water/oil mix

from the injection channel. This cemented the belief that the shoes are causing the shining band phenomenon and the steel particles from machining the bearings are increasing the severity of the shining band. This can be seen in Figure 4-10 where the shining band from the clean water/oil run is lighter than that of the shining band from the dirty water/oil mix run.

5.1.2 Numerical Conclusion

All numerical models were run with a constant gap between the bearing and the shoe, which does not accurately represent the experimental findings. Since the shoes touched down on the bearing surface during the experiments, it should be modeled in the numerical calculations. Even with the difference between the numerical and the experimental setups, the numerical models considered in this evaluation showed a reduction in the amount of steel entering the gap between the shoe and the bearing. The steel that makes is in the gap between the bearing and the shoe, although a very small quantity, could still cause the abrasions that lead to the shining band phenomenon. A stronger jet of clean coolant should be able to remove completely the steel particles from the gap between the bearing and the shoe.

5.2 Future Work

After reaching the aforementioned conclusion, there is room for improvement of the results of this research. In the next section some of the future work that can be done to better the results of both the numerical and experimental results.

5.2.1 Experimental Future Work

Different materials with different mechanical properties should be explored. Materials with different roughness and hardness react differently to rubbing against steel. A material that does not leave a mark on steel after rubbing is desired.

A stronger pump should be used to increase the flow of the lubricant through the shoe's injection channel to deflect more particles out of the small gap between the shoe and the rod.

5.2.2 Numerical Future Work

Numerically, modifications to the geometry of the shoe with the injection channel may be made to increase the effectiveness of the channel and increase the steel particles deflection. One possible change is the distance between the surface of the injection channel and the bearing. In the model created in this thesis, the distance between the injection channel surface to the bearing is 0.5 mm. Cutting that distance to 0.1 mm may result in reduction in steel particles entering the gap between the bearing and shoe. Also modeling the gap as a convergent divergent region that can generate lift force will be more realistic.

Appendix

A.1 Tables

Table A.1 Onyx material properties (31) (32)

Plastic Matrix	Onyx Material
Tensile Modulus (GPa)	1.4
Tensile Stress at Yield (MPa)	36
Tensile Strain at Yield (%)	25
Tensile Stress at Break (MPa)	30
Tensile Strain at Break (%)	58
Flexural Strength (MPa)	81
Flexural Modulus (GPa)	2.9
Heat Deflection Temp (˚C)	145
Melting Point (˚C)	215-128
Izod Impact – Notched (J/m)	330
Density (g/cm^3)	1.2

Table A.2 Mechanical properties of steel used in the experiments of this thesis (1018 steel) against steel used in the factory (HRC 60 bearing steel) (33) (34)

	1018 Steel	HRC 60 Bearing Steel
Density (g/cm^3)	7.87	7.86
Ultimate Tensile Strength (MPa)	440	431
Yield Tensile Strength (MPa	370	323
Young's Modulus (GPa)	205	206
Brinell Hardness	126	120
Specific Heat (kJ/kg.K)	0.486	0.48
Thermal Conductivity (W/m.K)	51.9	50

A.2 Figures

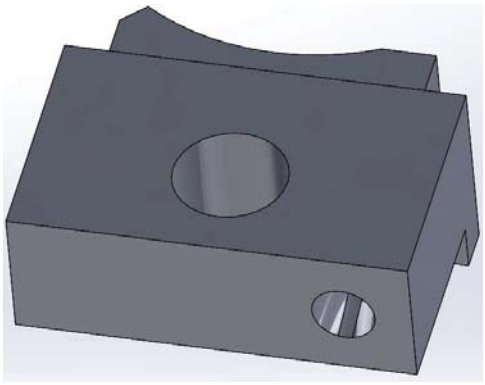

Figure A.1 a view of the circular cross-section of the shoe with fluid injection channel

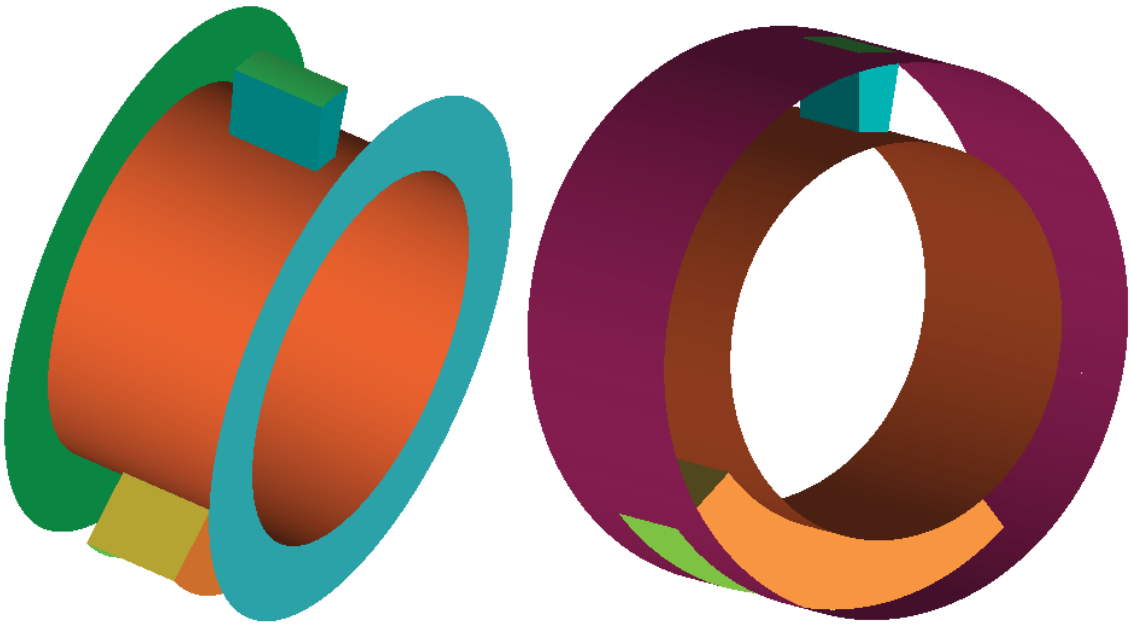

Figure A.2 isometric view of the three-dimensional model with side boundaries

References

1. *The Manufacturing of a Ball Bearing.* **bearingindustry.com.** 2017, p. pp 6.

2. *Study of the surface integrity of the machined workpiece in the EDM of tungsten carbide.* **Lee, Hiong and Li, Xiaoping.** 2003, Journal of Materials Processing Technology, Volume 139, p. pp 316.

3. *VR/Wesson - Hydro carbide.* **VanSteel.** 2009, p. pp 610.

4. **Seidelson, Dr. Craig.** *Manufacturing Process of Ball Bearings.* Canton, OH, 02 14, 2017.

5. *Progress in Additive Manufacturing and Rapid Prototyping.* **Kruth, J. P., Leu, M. L. and Nakagawa, T.** 1998, CIRP Annals Manufacturing Technology, pp. pp. 525-540.

6. *State of the Industry Report - Executive Summary.* **Wohlers, T.** 1998, Rapid Prototyping and Manufacturing Conference, pp. pp 951-962.

7. *Effect of Abrasive in Lubricant.* **McKee, S.A.** 1927, Journal of S.A.E Vol. 20, pp. pp. 3-6.

8. *Wear Reducing Additives for Lubricants Containing Solid Contaminants.* **Sharma, Subhash Chandra and Hargreaves, Doug.** 2008, p. pp 2.

9. *Performance of Oil-Film Bearings With Abrasive-Containing Lubricant.* **Roach, A.E.** 1951, Trans. ASME, Vol. 73, pp. pp. 677-686.

10. *Foreign Object Damage in Journal Bearings.* **Elwell, R.C.** 1978, Lubrication Engineering Vol. 34, pp. pp. 187-192.

11. *Wear of Bearing Liners at Low Speed Rotation of Shaft With Contaminated Oil.* **Wikström, V., Hoglund,, E. and Larsson, R.** 1993, Wear, Vol. 162-164, pp. pp. 996-1001.

12. *On the Scuffing Failure of Hydrodynamic Bearings in the Presence of an Abrasive Contaminant.* **Khonsari, M. M., Pascovici, M. D. and Kucinschi, B. V.** 1999, pp. pp. 1-7.

13. *Computational Fluid Dynamics Modeling of Gas-Liquid TwoPhase Flow around a Spherical Particle.* **Du, Wei, et al.** 2013, Chemical Engineering & Technology, pp. 840-850.

14. *Experimental and CFD study of unsteady airborne pollutant transport within an aircraft cabin mock-up.* **Yan, Wei, et al.** 2009, Building and Environment, pp. 34-43.

15. *CFD Modeling of Ash Deposition for Co-Combustion of MBM with Coal in a Tangentially Fired Utility Boiler.* **Taha, Taha, et al.** 2013, Fuel Processing Technology, pp. pp. 126-134.

16. *Simulation of Windblown dust transport from a mine tailings impoundment using a computational fluid dynamics model.* **Stovern, Michael, et al.** 2014, Aeolian Research Volume 14, pp. pp 75-83.

17. **Nagaraj, D.R.** *Minerals Recovery and Processing.* s.l. : John Wiley and Sons, 2005.

18. **Drummer, Dietmar, Cifuentes-Cuellar, Sandra and Rietzal, Dominic.** *Suitability of PLA/TCP for fused deposition modeling.* [Research Paper] Erlangen, Germany : Emerald Group Publishing Limited, 2013.

19. *CREATORBOT 3D Pro Series II specifications manual.* **3D-Printerworks.** 2018, pp. pp 1-2.

20. *ANSYS ICEM CFD User Manual.* **ANSYS ICEM CFD.** 2016.

21. *ANSYS ICEM CFD User Manual 14.5.* **ANSYS INC.** 2014, pp. pp 41-42.

22. **Nakayama, Y and Boucher, R. F.** *Introduction to Fluid Mechanics.* Jordan Hill : Butterworth-Heinmann, 1999.

23. **Smits, Alexander.** *A Physical Introduction to Fluid Mechanics.* Princeton : Princeton University, 2017.

24. **ANSYS INC. .** ANSYS FLUENT User's Guide. s.l. : ANSYS INC., 2017.

25. **Stephen, Dr. T.** *Solubilities of inorganic and organic compounds.* Kronberg-Taunus : Pergamon Press, 1963.

26. *ANSYS THEORY GUIDE.* **ANSYS.** s.l. : ANSYS, 2017.

27. **Harnoy, Avraham.** *Bearing Design in Machinery.* New York : Marcel Dekker, 2003.

28. **Arfken, G.** *Mathematical Methods for Physicists.* Orlando : Academic Press, 1985.

29. **Kuron, Mike.** 3 Criteria for Assessing CFD Convergence. *Engineering.com.* [Online] January 6, 2015. [Cited: March 9, 2018.] https://www.engineering.com/DesignSoftware/DesignSoftwareArticles/ArticleID/9296/3-Criteria-for-Assessing-CFD-Convergence.aspx.

30. **Cohen, Richard, et al.** *Quantities, Units and Symbols in Physical Chemistry.* Cambridge : International Union of Pure and Applied Chemistry, 2007.

31. **Markforged.** Material Specifications Composites. *Markforged.com.* [Online] 2018. [Cited: 03 19, 2018.] https://static.markforged.com/markforged_composites_datasheet.pdf.

32. —. Onyx Safety Data Sheet. *markforged.com.* [Online] 05 04, 2016. [Cited: 04 10, 2018.] https://www.advantagelitho.com/amfilerating/file/download/file_id/94/.

33. **NSK.** bearing materials. *NSK.com.* [Online] 04 05, 2018. [Cited: 04 05, 2018.] http://www.nsk.com.br/upload/file/nsk_cat_e728g_10.pdf.

34. **AZOM.** AZOM Materials. *AZOM.com.* [Online] 07 05, 2012. [Cited: 04 05, 2018.] https://www.azom.com/article.aspx?ArticleID=6115.

35. *LULZBOT TAZ 6* . **LULZBOT.** 2018, p. 1.

36. **eBay.** eBay.com. *Kingsbury Shoe Thrust.* [Online] Kingsbury inc., 03 14, 2018. [Cited: 03 14, 2018.] https://www.ebay.com/itm/262335219128?rmvSB=true.

37. **NSBEARINGS FAQ.** ***NSBEARINGS.com.*** **[Online] NS BEARINGS, 03 14, 2018. [Cited: 03 14, 2018.] 2018.**